Design of a Fractal Antenna Based on Hexaflake Fractal Structure

by

Sajid Muhaimin Choudhury

Master of Science in Electrical and Electronic Engineering

Department of Electrical and Electronic Engineering

Bangladesh University of Engineering and Technology

November 2011

The thesis entitled "**Design of a Fractal Antenna Based on Hexaflake Fractal Structure**" submitted by Sajid Muhaimin Choudhury, Roll No: 1009062044, Session: October 2010 has been accepted as satisfactory in partial fulfillment of the requirements for the degree of Master of Science in Electrical and Electronic Engineering on 16 November 2011

BOARD OF EXAMINARS

1. **Chairman**
(Supervisor)

Dr. Md. Abdul Matin
Professor
Department of Electrical and Electronic Engineering
Bangladesh University of Engineering and Technology
Dhaka – 1000

2. **Member**
(Ex-officio)

Dr. Md. Saifur Rahman
Professor and Head of the Department
Department of Electrical and Electronic Engineering
Bangladesh University of Engineering and Technology
Dhaka – 1000

3. **Member**

Dr. Pran Kanai Saha
Professor
Department of Electrical and Electronic Engineering
Bangladesh University of Engineering and Technology
Dhaka – 1000

4. **Member**
(External)

Dr. A B M Siddique Hossain
Professor and Dean
Faculty of Engineering
American International University-Bangladesh (AIUB)
Dhaka – 1212

Candidate's Declaration

It is hereby declared that this thesis or any part of it has not been submitted elsewhere for the award of any degree or diploma and that all sources are acknowledged.

Signature of the Candidate

Sajid Muhaimin Choudhury

Dedication

I would like to dedicate this thesis to my loving parents ...

Acknowledgements

First and foremost, I would like to express my sincere and deepest gratitude to Almighty Allah for giving me the ability and strength to complete this research work.

I express my deepest gratitude to Prof. Dr. Md. Abdul Matin for his kind supervision, guidance and constant support in completing my research presented in this thesis. Without his valuable guidance, the research would not have been possible.

I would like to thank Prof. Dr. Md. Saifur Rahman, Professor and Head of the Department for sharing his precious time in reviewing my thesis work. My gratitude and thanks to Prof. Dr. Pran Kanai Saha and to Prof. Dr. A B M Siddique Hossain for their kind consent to evaluate my thesis.

I would like to acknowledge the encouragement and support of my parents. Without their mental support it would not have been possible to make a successful completion of the thesis.

Abstract

Design of a fractal antenna structure based on iteration 1 and iteration 2 of hexaflake fractal structure is proposed. A multiport network model of basic hexagonal patch structure is analysed. Based on hexagonal structure two hexaflake fractal structures are designed. The resulting patch structure provides a way to significantly reduce the patch antenna size and increase bandwidth over rectangular patch structure. Effects of changing coupling width and substrate thickness on fractals have been studied. The designed antenna is based on simple printed circuit technology and can be readily constructed using low cost FR-4 substrate material. The hexagonal element showed reduction of bandwidth and reduced resonance frequency compared to rectangular patch antenna. The first iteration of hexaflake fractal results in a 46.92% reduction of patch area compared to hexagonal patch element. The second iteration of hexaflake fractal patch element results in 18.5% reduction of patch area compared to the first iteration of hexaflake fractal, and 56.74% reduction of patch area compared to the hexagonal patch. Thus the fractal structures clearly demonstrate ability to reduce patch size for operation at a higher frequency.

Contents

Board of Examinars i

Declaration ii

Dedication iii

Acknowledgement iv

Abstract v

Contents vi

List of Figures x

List of Tables xiii

Nomenclature xv

1 Introduction 1

1.1 Introduction . . . 2

1.1.1 Fractal Structure . . . 2

1.1.2 Hexaflake Fractal . . . 3

1.2 Literature Review . . . 3

1.3 Objective of the Present Work . . . 5

1.4 Thesis Outline . . . 5

2 Theory 7

2.1 Introduction . . . 8

2.2 Antenna Terms . . . 8

2.2.1 Radiation Pattern . . . 8

2.2.1.1 Normalized Field Pattern . . . 8

2.2.1.2 Half Power Beam Width . . . 9

2.2.2 Directivity . . . 9

2.2.3 Bandwidth . . . 9
2.2.4 Input Impedance . . . 10
2.2.5 Antenna Radiation Efficiency . . . 10
2.3 Microstrip Patch Antenna . . . 10
2.3.1 Antenna Structure . . . 11
2.3.2 Antenna Feed . . . 11
2.3.2.1 Coaxial Feed . . . 12
2.3.2.2 Microstrip line Feed . . . 12
2.3.3 Method of Analysis . . . 13
2.3.3.1 Transmission Line Model . . . 13
2.3.3.2 Cavity Model . . . 13
2.3.3.3 Finite Element Method . . . 14
2.4 Network Analysis . . . 14
2.4.1 Equivalent Current and Voltages . . . 14
2.4.2 Multiport Network . . . 15
2.4.3 Scattering Parameter . . . 16
2.4.3.1 Reflection Coefficient . . . 17
2.4.3.2 Transmission Coefficient . . . 17
2.5 Basic Hexagonal Patch Antenna . . . 18
2.5.1 Equivalent Sources of the Hexagonal Patch . . . 19
2.6 Radiation Conductance of Hexagonal Patch . . . 19
2.7 Conclusion . . . 22

3 Multiport Analysis of Hexagonal Patch 23
3.1 Introduction . . . 24
3.2 Mathematical Derivation . . . 24
3.2.1 Segmentation Method . . . 24
3.2.2 Z-matrix for basic rectangular and triangular segments . . . 25
3.2.3 Segment joining to form Z-Parameter matrix of an unloaded hexagonal patch . . . 28
3.2.4 Modeling Radiation of Hexagonal Patch . . . 29
3.3 Multiport Analysis of a Hexagonal Patch . . . 32
3.4 Conclusion . . . 32

4 Simulation of Hexagonal Patch 33
4.1 Introduction . . . 34
4.1.1 Antenna Substrate . . . 34
4.2 Modelling of Coaxial Feed . . . 34
4.2.1 Resonance for different patch size . . . 35

4.2.1.1 Center Frequency at different values of sidelength, a 36
4.2.1.2 Bandwidth at different values of sidelength, a . . . 36
4.2.2 Comparison with simulation results of a rectangular patch . 37
4.3 Conclusion . . . 38

5 First Iteration of Hexaflake Patch 39
5.1 Introduction . . . 40
5.2 Patch Structure . . . 40
5.3 Effect of Changing Coupling Width . . . 40
5.4 Varying the Side Length of Center-fed First Iteration of Hexaflake . 43
5.5 Optimum Feed Position . . . 44
5.6 Effect of Substrate Thickness . . . 46
5.7 Conclusion . . . 49

6 Second Iteration of Hexaflake Patch 50
6.1 Introduction . . . 51
6.2 Patch Structure . . . 51
6.3 Effect of Changing Coupling Width . . . 51
6.4 Optimal Feed Position . . . 53
6.5 Varying Patch Size . . . 56
6.6 Conclusion . . . 58

7 Effect of FSS Ground Plane 59
7.1 Introduction . . . 60
7.2 Frequency Selective Surface . . . 60
7.3 Array of Four legged loaded element . . . 62
7.4 Second Iteration of Hexaflake Patch with FSS Ground Plane . . . 64
7.5 Conclusion . . . 65

8 Results and Discussion 66
8.1 Introduction . . . 67
8.2 Performance of Designed Antenna . . . 67
8.2.1 As a Hexagonal Patch . . . 67
8.2.2 As a First Iteration of Hexaflake Patch . . . 69
8.2.3 As a Second Iteration of Hexaflake Patch . . . 71
8.3 Comparison of Performance . . . 73
8.3.1 Return Loss . . . 73
8.3.2 Parameters of Antenna . . . 73
8.4 Comparison with other fractal structures . . . 74
8.5 Conclusion . . . 75

9 Conclusions **76**

9.1 Concluding Remarks 77

9.2 Recommendation for Future Work 77

References **78**

List of Figures

1.1 Generation of Sierpinski Triangle 2
1.2 Generation of Hexaflake Fractal 3

2.1 Basic Radiation Pattern of an Antenna 9
2.2 Patch Antenna 11
2.3 Microstrip Feed 12
2.4 Field distribution at arbitrary two conductor transmission line . . . 15
2.5 Basic Hexagonal Patch 18
2.6 Single Slot of a Hexagonal Patch 20

3.1 (a) Basic Hexagonal Structure (b) Structure divided into triangles and rectangle (c) Multiport Representation of a hexagonal patch . 24
3.2 (a) Segmentation of unloaded hexagonal patch into part A, B, C, D, E(b) Joining part A and B 29
3.3 Edge Admittance Network 30
3.4 Loaded Hexagonal Patch Multiport Model 30

4.1 Coaxial Feed Model 34
4.2 Simulation of Basic Hexagonal Patch 35
4.3 Return loss of basic hexagonal patch at different values of a 35
4.4 Center Frequency of First Band of basic hexagonal patch at different values of a 36
4.5 Return Loss Bandwidth of First Band of basic hexagonal patch at different values of a 37
4.6 Center Frequency of first band vs basic hexagonal patch and rectangular patch at different values of a 37
4.7 RL Bandwidth of first band vs basic hexagonal patch and rectangular patch at different values of a 38

5.1 First Iteration of Hexaflake Structure 40
5.2 Coupling width with scaling factor cs 41
5.3 Iteration of Fractal Structure with $cs = 4$ 41

5.4 Return loss for varying coupling width 42
5.5 Change of center frequency for varying individual port lengths . . . 42
5.6 Return loss of first iteration of hexaflake structre patch with variation of patch size 43
5.7 Center frequency of first iteration of hexaflake patch structure with variation of patch size 44
5.8 Variation of feed position of the first iteration of hexaflake patch . . 45
5.9 Return loss for Varying feed position of the first iteration of hexaflake patch 45
5.10 Increasing Layer thickness for first iteration hexaflake 47
5.11 Return loss for triple substrate thickness for first iteration hexaflake 47
5.12 Change of RL Bandwidth with substrate thickness 48

6.1 Second Iteration of Hexaflake Structure 51
6.2 Second Iteration of Hexaflake Structure with extended port width . 52
6.3 Return loss of Second Iteration Hexaflake by varying coupling width 52
6.4 Varying coupling width of Second Iteration Hexaflake 53
6.5 Varying feed position of the second iteration of hexaflake patch . . . 54
6.6 Return loss for varying feed position of the second iteration of hexaflake patch 55
6.7 Return loss for varying fractal size of the second iteration of hexaflake patch 56
6.8 Center Frequencies of the operating bands of the second iteration of hexaflake patch 57
6.9 Percent RL Bandwidth of the operating bands of the second iteration of hexaflake patch 57

7.1 Basic Principle of Frequency Selective Surface 60
7.2 Four Legged Loaded Element as FSS 61
7.3 Array of loaded element on FR4 substrate 62
7.4 Transmission Coefficient of array of loaded element on FR4 substrate 63
7.5 Transmission Coefficient of array of loaded element on FR4 substrate 63
7.6 Simulation of Second Iteration of Hexaflake Patch with FSS Ground Plane 64
7.7 Simulation of Second Iteration of Hexaflake Patch with FSS Ground Plane 65

8.1 Return loss for designed Basic Hexagonal Patch 67
8.2 Radiation pattern of designed Basic Hexagonal Patch 68
8.3 3D Radiation pattern of designed Basic Hexagonal Patch 68

8.4 Return loss for designed First Iteration of Hexaflake Patch 69
8.5 Radiation pattern of designed First Iteration of Hexaflake Patch . . 70
8.6 3D Radiation pattern of designed First Iteration of Hexaflake Patch 70
8.7 Return loss for designed Second Iteration of Hexaflake Patch 71
8.8 Radiation pattern of designed Second Iteration of Hexaflake Patch . 72
8.9 3D Radiation pattern of designed Second Iteration of Hexaflake Patch 72
8.10 Return loss for three designed antennas 73

List of Tables

4.1 Properties of FR-4 Substrate 34

5.1 First iteration hexaflake fractal patch antenna center frequency and RL Bandwidth 46
5.2 Increased substrate thickness first iteration hexaflake center frequency and RL Bandwidth 48

6.1 Frequency Bands obtained by varying feed position in second iteration of hexaflake 55

8.1 Comparison of the designed antennas 74
8.2 Comparison of second iteration of hexaflake patch with other published results 75

Nomenclature

Roman Symbols

a	length of the side of a hexagon
cs	Coupling Scaling Factor
f_c	Center Frequency
λ_0	Free space frequency
G	Radiation Conductance
J	Electric Current Density
M	Magnetic Current Density
R_A	Radiation Resistance
S_{11}	Reflection Coefficient
S_{21}	Transmission Coefficient
Z_ij	Z parameter between port i and j

Greek Symbols

δ	Loss Tangent
ϵ	Electric Permittivity of Medium
η	Radiation efficiency
μ	Magnetic Permeability of Dielectric Medium
ω	Angular Frequency

Acronyms

BW	Band Width

EAN Edge Admittance Network

FEM Finite Element Method

FSS Frequency Selective Surface

GPS Global Positioning System

MSA Microstrip Antenna

RL Return Loss

Z_A Antenna Input Impedance

Chapter 1

Introduction

1.1 Introduction

1.1.1 Fractal Structure

A special type of rough or fragmented geometric definition that is iterative, in a sense that it itself can be split into reduced size copies of itself is called a fractal [1]. Fractals are self-similar and independent of scale. Fractals can describe many real-life objects occurring in the nature, such as plant leaves, snow flakes, clouds, mountains, turbulence, and coastlines that do not correspond to simple geometric shapes. The origins of fractal theories can be traced back to Helge von Koch in 1904 [2]. Waclaw Sierpinski gave the concept Sierpinski triangle in 1915, example of which is shown in Figure 1.1. Mandelbrot coined the terms fractal and fractal dimension in 1983.

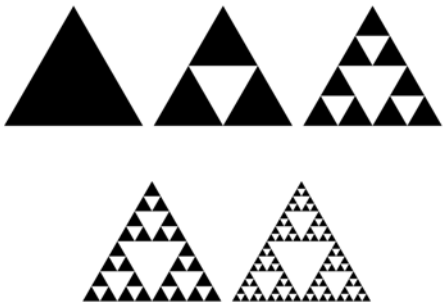

Figure 1.1: Generation of Sierpinski Triangle

After a span of ninety years fractals came to renewed interest to electromagnetic research. Fractal concepts were first introduced in modified monopole antennas to reduce their dimension. Introducing fractal geometry in antenna can be employed both as a multiband solution and also as a method to reduce size, as the antenna is self similar and the properties at smaller size can be employed to obtain multi-band operation. Fractal structure itself incorporates various bends or holes that act as lumped or continuous loading elemenets [3]. This enables to avoid multiple capacitor and inductor coils and loading with pure shaping alone.

Some of the main advantages of fractal structure include:

- Broadband and multiband frequency response that is derived from the self similar geometric structure
- Compact size compared to similar conventional antenna designs with good to excellent efficiencies and gain

- Simplicity in construction, as no discrete components are required to construct the antenna to match impedance
- Multifrequency characteristics design with specified stop band and multiple specific passbands.

1.1.2 Hexaflake Fractal

A special case of Sierpinski N-Gons fractal structure [4] is a geometrical hexaflake fractal structure, which is based on hexagons.

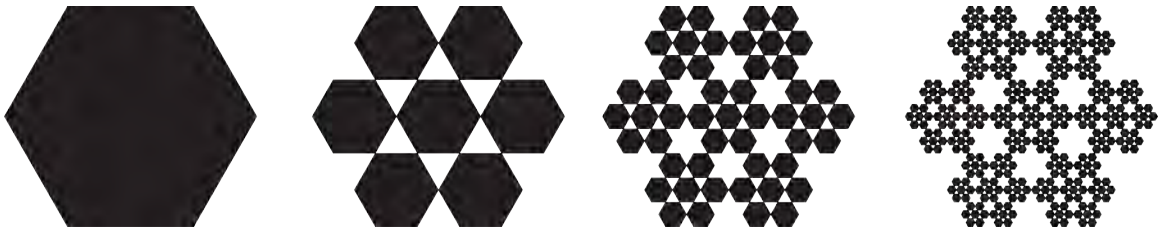

Figure 1.2: Generation of Hexaflake Fractal

1.2 Literature Review

The fractal antenna was proposed by Puente et al. [5] based on Sierpinski gasket. Different types of fractal slot antenna has since been studied such as, Koch Fractal Antenna [6], the Pythagoral Fractal Antenna [7], Appollian Gasket Fractal Antenna [8], modified Sierpinski gasket [9], modified Minkowski Fractal [10], hybrid Koch-Sieponski fractal [11], Inverted Koch Square Fractal [12], combined Giusepe Peano.

- Sierpinski gasket studied by Puente et al. [5] found multiband operation using the self similar triangular structure of Sierpinski triangles.
- Hazdra et al. [12] proposed a miniature fractal patch antenna based on Lindenmayer System fractal generators . The proposed structure makes it possible for 20% miniaturization of the fractal structure compared to the rectangular patch.
- Modified Sierpinski gasket slot proposed by Mahatthanajatuphat and Akkaraekthalin [9] enables multiband operation of antenna with multiband operation at DCS (1.71 - 1.88 GHz), WiMAX (3.3 - 3.8 GHz), IMT advance system or 4G mobile communication system (3.4 - 4.2 GHz), and WLAN IEEE 802.11a (5.15 - 5.35 GHz) bands.

- Tiwari and Kumar [8] proposed Appollian Gasket Monopole Fractal Antenna fabricated using printed circuit technology on FR4 substrate, with multiple bands at 1.12 GHz, 4.65 GHz and 7.75 GHz with bandwidth of 50%, 19.5% and 15% respectively . The experimental radiation pattern of antenna is omni-directional at lower frequency and like electric dipole at higher frequency.

- Mahatthanajatuphat et al. [10] proposed a Modified Minkowski Fractal antenna for multiband operation . They also proposed a modification of the ground plane for the monopole and found the antenna to be appropriate for PCS 1900 (1.85-1.99 GHz), UMTS (1.92-2.17 GHz), WLAN (2.40-2.48 GHz/5.15-5.35 GHz/5.725-5.825 GHz), Mobile WiMAX (2.3-2.36 GHz/2.5-2.69 GHz), and WiMAX (5.25-5.85 GHz) with omnidirectional radiation pattern.

- Kim et al. [6] proposed the Koch Fractal Patch Antenna . The proposed Koch Fractal Patch Antenna could exploit the space filling properties of fractal geometry and experimentally could reduce the patch size by 45% by using an iteration factor of 2.5.

- Prombutr et al. [13] proposed a Hilbert curve fractal antenna feed for coplanar waveguide. They proposed a numerical model for analysis of fractal geometry based on transmission line model.

- Aggarwal and Kartikeyan [7] proposed the Pythagoras Tree fractal patch antenna for multi-frequency use, essentially repeating a simple rectangular patch structure by Pythagoras Tree. The resulting patch antenna could operate simultaneously in 2.15-2.75 GHz for the lower band centered at 2.35 GHz and 3.1-4.2875 GHz for the higher band centered at 3.54 GHz, which are designated operation frequency of both WLAN and WiMAX.

- Oliveria et al. [14] proposed a compact first iteration Koch fractal patch antenna on an EBG Ground plane. The designed antenna yields better return loss bandwidth compared to non-EBG antenna.

- Tiwari and Kartikeyan [15] synthesized a basic rectangular patch structure which incorporated a fractal shaped defect. By increasing the current paths in the patch, a size reduction of 67% was possible.

- Chakraborty et al. [16] showed that the increased current path produced by slots in a rectangular patch can reduce the resonant frequency of the patch.

- Yu et al. [11] proposed a combination of Koch and Sierpinski fractal shapes as a patch shape for a microstrip antenna. They inserted a Sierpinski carpet into a single patch and etched the inner and outer patch edges with Koch curves. The resonant frequency significantly reduced as the iteration order of the patch was increased.

Literature study shows that a Hexaflake fractal structure has not yet been studied as a patch antenna [6–16] . Simple hexagonal patch antenna has potential to essentially increase impedance bandwidth up to 6% [17] compared to a rectangular patch antenna, which is the basis for fore-mentioned fractals [6, 7, 9–12]. It can thus be expected that the hexaflake fractal structure would have better radiation characteristics compared to the previous fractal structures. The proposed hexaflake structure is geometrically iterative as a fractal [4], and thus can be exploited to have multiple band operation of a fractal patch antenna.

1.3 Objective of the Present Work

The objective of this thesis work is to

i. Study the properties of a simple hexagonal patch antenna and model the input impedance of the antenna with closed formed equations

ii. To study the effect of different level of hexaflake fractal on the performance of the antenna

iii. To study effect of modifying the ground plane of the antenna

iv. To compare the proposed hexaflake structure with different types of published antenna structures

1.4 Thesis Outline

This thesis has 9 Chapters.

- After this Introductory chapter, Chapter 2 covers some of the fundamental theories related to a patch antenna and analysis used in the thesis work. Also the concept of slot radiator in modelling microstrip antennas is introduced which is used to calculate radiation conductance of a basic hexagonal patch antenna.

- In chapter 3, an extended multiport analysis method for hexagonal patch antenna is proposed. The proposed model is used to calculate the voltage distribution of the patch and thus the far field radiation pattern.

- In chapter 4, the performance of hexagonal patch is discussed based on computer simulation performed using the High Frequency Simulation Software (HFSS) from Ansoft.
- In chapter 5, the performance of the first iteration of hexaflake fractal structure is evaluated as a patch antenna structure.
- In chapter 6, the performance of the second iteration of hexaflake fractal structure is evaluated as a patch antenna structure.
- In chapter 7, the effect of adding a Frequency Selective Surface (FSS) ground plane is studied for patch antenna structures.
- In chapter 8, the results and major findings of this thesis are analysed.

Lastly, a summary of the contributions regarding the work done in this thesis and scope of future research work is described to conclude the thesis.

Chapter 2

Theory

2.1 Introduction

This chapter covers some of the fundamental concepts regarding patch antenna and analysis of such antenna systems. At first some generalized terms regarding basic antenna systems are discussed, afterwards, a brief introduction regarding patch antenna and methods of analysis of patch antenna is given. Afterwards, some concepts regarding analysis of patch antenna such as scattering matrix and impedance matrix is discussed that is applied later in the thesis. the fundamental component of the Hexaflake structure is discussed. The basic hexagon is used as a patch substrate. The transmission line of hexagonal patch is proposed from which the radiation conductance of the hexagonal patch element is derived.

2.2 Antenna Terms

A radio antenna is a structure associated with the transition of an electromagnetic wave from a guided medium to free space. From circuit point of view antennas appear in a transmission line as a resistance called Radiation Resistance (R_r)

2.2.1 Radiation Pattern

The radiation pattern of an antenna is the three dimensional quantity associated with the variation of field power as a function of spherical coordinates. To completely specify the radiation pattern of an antenna, the components of electric field in spherical coordinates, $E_\theta(\theta, \phi)$ and $E_\phi(\theta, \phi)_n$ and the phase angle of the fields $\delta(\theta, \phi)$ needs to be known.

A field pattern is presented in three dimensional spherical coordinates or by cut planes through main lobe axis. A typical antenna field pattern is shown in Figure 2.1. Two field patterns at right angle are called principal plane patterns. If the antenna field pattern is symmetric, only one principal pattern obtained from cutting the three dimensional radiation pattern from a plane, is sufficient. [18]

2.2.1.1 Normalized Field Pattern

Normalized field pattern is defined as

$$E_\theta(\theta, \phi)_n = \frac{E_\theta(\theta, \phi)}{E_\theta(\theta, \phi)_{max}} \tag{2.1}$$

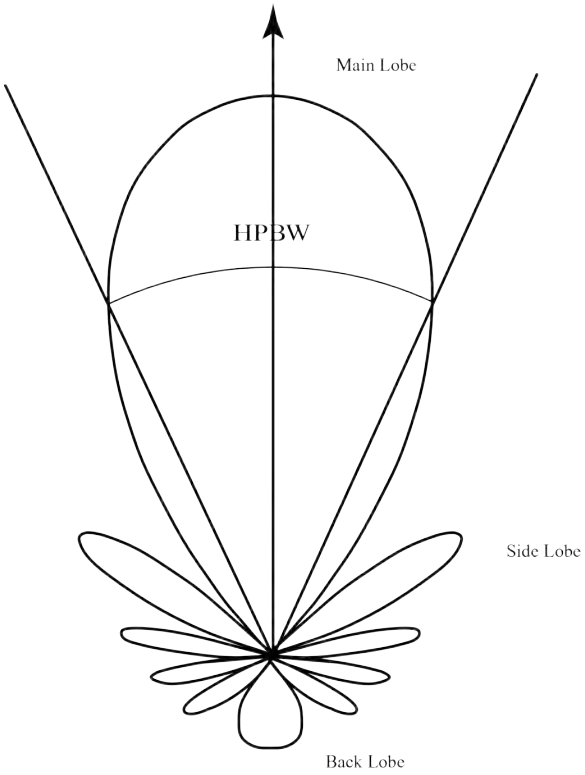

Figure 2.1: Basic Radiation Pattern of an Antenna

2.2.1.2 Half Power Beam Width

The half power beam width of an antenna is defined as the angular width between the two -3dB points in the field pattern of an antenna with respect to the normalized main lobe.

2.2.2 Directivity

The radiation intensity of an antenna is defined as the power radiated from an antenna per unit solid angle. The ratio of radiation intensity in a given direction from the antenna to the radiation intensity averaged over all directions is called the directivity of the antenna.

2.2.3 Bandwidth

The bandwidth of an antenna is defined as the range of frequency in which the antenna performance, with respect to some given characteristics that conforms to a particular standard. Bandwidth is usually considered as a range of frequencies on both sides of a center frequency. Characteristics of antenna can be denoted in terms of input impedance, pattern, gain, polarization etc. Bandwidth is often

defines as a percentage using the following equation,

$$\%BW = \frac{f_H - f_L}{f_C} \times 100\% = \frac{f_H - f_L}{f_H + f_L} \times 200\% \tag{2.2}$$

where f_H and f_L is the higher and lower frequency limit between which the conditions is met, and $f_C = (f_H + f_L)/2$ is the center frequency or the resonance frequency.

2.2.4 Input Impedance

Input impedance of an antenna is defined as the impedance presented by an antenna at the terminals of the antenna. Input impedance has two components:

$$Z_A = R_A + jX_A \tag{2.3}$$

where R_A is the antenna input resistance and X_A is the antenna input admittance. R_A can be divided in to two parts.

$$R_A = R_r + R_L \tag{2.4}$$

where R_r is the antenna radiation resistance and R_L is the loss resistance.

2.2.5 Antenna Radiation Efficiency

Radiation efficiency of an antenna is approximated as the ratio of total power input to the antenna and the power dissipated by the radiation resistance.

$$\eta = \frac{R_r}{R_r + R_L} \tag{2.5}$$

2.3 Microstrip Patch Antenna

Microstrip Patch antennas are widely used for their low profile characteristics. They are electrically thin, light weight, easy to fabricate and low cost antenna. The performance of a microstrip antenna suffers from various drawbacks, such as narrow bandwidth, high feed network losses, high cross polarization and low power handling capacity [19].

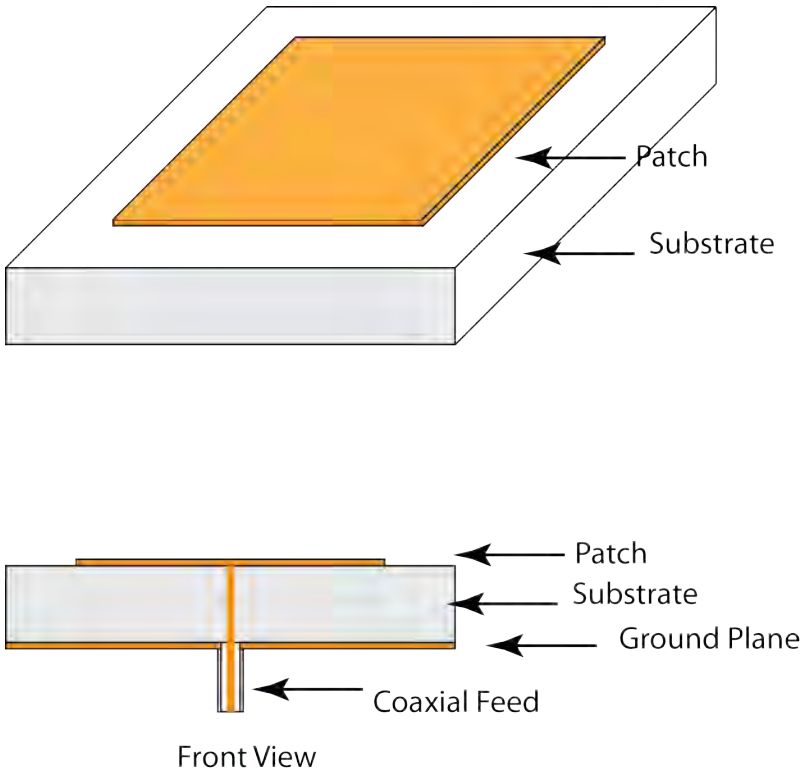

Figure 2.2: Patch Antenna

2.3.1 Antenna Structure

The basic patch antenna structure is shown in Figure 2.2. The antenna is fed with a Coaxial probe feed or a planar microstrip line. A planar geometrical structure is used as the patch. Elementary Square patch, Circular, Triangular, Pentagonal and Annular shapes are reported by James et al. [20] The patch is formed on a dielectric substrate, and backed by a ground plane. The substrate of the antenna has usually a dielectric constant of $2.2 < \epsilon_r < 10$, where ϵ_r is relative dielectric constant. The substrate whose size is thick and dielectric constant is in the range of lower end provides better efficiency and bandwidth; but it expenses large element size.

2.3.2 Antenna Feed

There are several feeding methods available to feed the electromagnetic wave into a microstrip antenna. Most popular techniques include coaxial probe, microstrip line aperture coupling and proximity coupling.

2.3.2.1 Coaxial Feed

The Coaxial feed is widely used for feeding a patch antenna. Coaxial cable is formed by an inner conductor surrounded by insulating material and again surrounding by a conducting cylinder that act as ground. As seen from Figure 2.2, the inner conductor of a coaxial connector is extended beyond the dielectric substrate of the antenna and is soldered to the radiating patch, while the outer conductor is connected to the ground plane. The main advantage of this type of feeding scheme is that the feed can be placed at any desired location inside the patch in order to match with its input impedance. Coaxial feed method is easy to implement and has low spurious radiation. However, its major disadvantage is that it provides narrow bandwidth and is difficult to model since a hole has to be drilled in the substrate and the connector protrudes outside the ground plane, thus not making it completely planar for thick substrates ($d > 0.02\lambda_0$). Also, for thicker substrates, the increased probe length makes the input impedance more inductive, leading to matching problems.

2.3.2.2 Microstrip line Feed

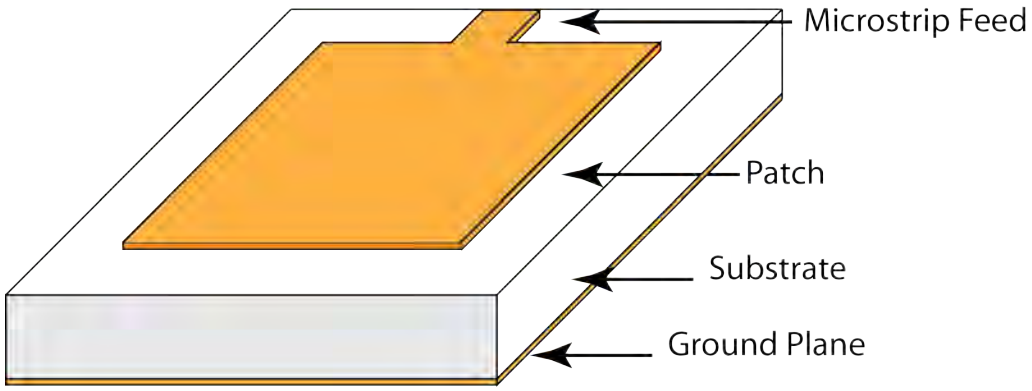

Figure 2.3: Microstrip Feed

In stripline feed, a conducting strip is connected directly to the edge of the Microstrip patch as shown in Figure 2.3. The conducting strip is smaller in width as compared to the patch and this kind of feed arrangement has the advantage that the feed can be etched on the same substrate to provide a planar structure. The purpose of the inset cut in the patch is to match the impedance of the feed line to the patch without the need for any additional matching element. This is achieved by properly controlling the inset position. Hence this is an easy feeding scheme, since it provides ease of fabrication and simplicity in modeling as well as impedance matching. However, as the thickness of the dielectric substrate being

used increases, surface waves and spurious feed radiation also increases, which hampers the bandwidth of the antenna. The feed radiation also leads to undesired cross polarized radiation. The feed position is also limited to the side of the patch as opposed to the freedom of feed point selection in Coaxial feed.

2.3.3 Method of Analysis

Two particular models are developed to explain microstrip antenna operation - transmission line model and cavity model, and also Full Wave method of analysis is used to find out characteristics of Microstrip Antennas. [21]

2.3.3.1 Transmission Line Model

The transmission line model of a microtrip antenna is simple to understand and also helpful to use for the basic performance. The model is not so accurate compared to other methods. A microstrip radiator element is modelled as a transmission line resonator. The transverse field variations are ignored thus the field only varies along the length, and the radiation occurs mainly from the fields at the open circuited ends that are poured outside (fringing fields). The patch is represented by two slots that are spaced by the length of the resonator. The model was originally developed for rectangular patches but has been extended for generalized patch shapes. Although the transmission line model is easy to use, all types of configurations can not be analyzed using this model since it does not take care of variation of field in the orthogonal direction to the direction of propagation.

2.3.3.2 Cavity Model

In the cavity model, the region between the patch and the ground plane of a microstrip antenna is modelled as a resonating cavity that is surrounded by magnetic walls around the periphery and by electric walls from the top and bottom sides. The model works well for thin substrates, as the field inside the cavity is uniform along the thickness of the substrate. The fields underneath the patch for regular shapes such as rectangular, circular, triangular, and sectoral shapes can be expressed as a summation of the various resonant modes of the two-dimensional resonator.

The fringing fields that extend from the patch periphery are treated by extending the patch boundary outward so that the effective dimensions are larger than the physical dimensions of the patch. The effect of the radiation from the antenna and the conductor loss are accounted for by adding these losses to the loss tangent of the dielectric substrate. The far field and radiated power are computed from the equivalent magnetic current around the periphery. An alternate way of incor-

porating the radiation effect in the cavity model is by introducing an impedance boundary condition at the walls of the cavity. The fringing fields and the radiated power are not included inside the cavity but are localized at the edges of the cavity.

2.3.3.3 Finite Element Method

In Finite Element Method (FEM), the region of interest is divided into any number of finite surfaces or volume elements depending upon the planar or volumetric structures to be analyzed. The smaller discrete elements are generally referred to as finite elements. These can be any well-defined geometrical shapes such as triangular elements for planar configurations and tetrahedral and prismatic elements for three-dimensional configurations, which are suitable even for curved geometry. It involves the integration of certain basis functions over the entire conducting patch, which is divided into a number of subsections. The problem of solving wave equations with inhomogeneous boundary conditions is tackled by decomposing it into two boundary value problems, one with Laplace's equation with an inhomogeneous boundary and the other corresponding to an inhomogeneous wave equation with a homogeneous boundary condition. Various software solutions exist commercially to realize finite element solutions of different types of antenna structures.

2.4 Network Analysis

2.4.1 Equivalent Current and Voltages

For an arbitrary two conductor transmission line shown in Figure 2.4, if the electric field **E** and and magnetic field **H** is known, the voltage V and current I associated with **E** and **H** can be obtained from

$$V = \int_{+}^{-} \mathbf{E} \cdot dl \tag{2.6}$$

and

$$I = \oint_{C+} \mathbf{H} \cdot dl \tag{2.7}$$

where in Equation 2.6 the integration is from + conductor to − conductor, and in Equation 2.7 the integration contour is a closed path enclosing the + conductor. Consequently, if the equivalent voltage and current of the two substrates are known, the electric and magnetic fields can be determined.

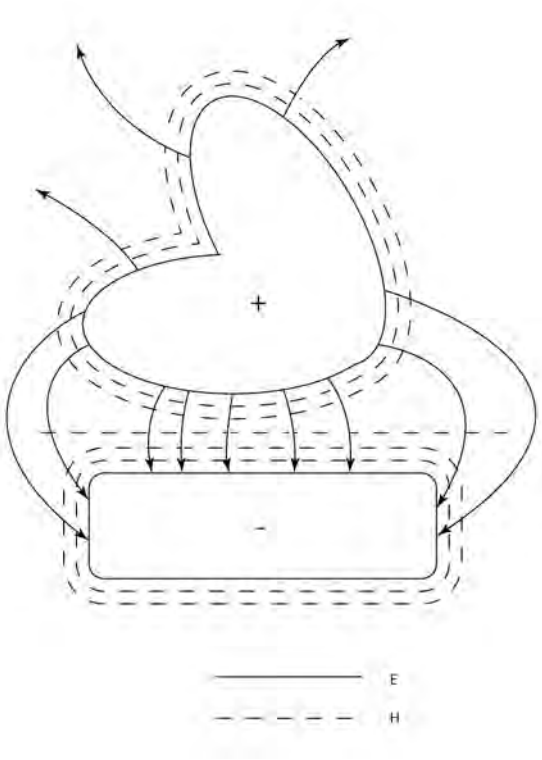

Figure 2.4: Field distribution at arbitrary two conductor transmission line

2.4.2 Multiport Network

The concept of equivalent network can be further extended to a multiport microwave network where the ports are transmission line or equivalent of transmission lines.

For an arbitrary N port microwave network, at any particular nth port, a terminal plane is assumed where the terminal plate experiences some incident and reflected waves. The incident and reflected waves can be converted into equivalent current and voltage sources as per Equation 2.6 and 2.7. Let, for incident voltage, the values are (V_n^+, I_n^+) and for reflected waves (V_n^-, I_n^-). So at the terminal plane, the voltage and currents can be given by,

$$V_n = V_n^+ + V_n^- \tag{2.8}$$

$$I_n = I_n^+ + I_n^- \tag{2.9}$$

The impedance matrix $[Z]$ of the microwave network can then be defined as,

$$\begin{bmatrix} V_1 \\ V_2 \\ \vdots \\ V_N \end{bmatrix} = \begin{bmatrix} Z_{11} & Z_{12} & \dots & Z_{1N} \\ Z_{21} & & & \vdots \\ \vdots & & & \vdots \\ Z_{N1} & \dots & \dots & Z_{NN} \end{bmatrix} \begin{bmatrix} I_1 \\ I_2 \\ \vdots \\ I_N \end{bmatrix} \tag{2.10}$$

where

$$[Z] = \begin{bmatrix} Z_{11} & Z_{12} & \dots & Z_{1N} \\ Z_{21} & & & \vdots \\ \vdots & & & \vdots \\ Z_{N1} & \dots & \dots & Z_{NN} \end{bmatrix} \tag{2.11}$$

Similarly, admittance matrix can be defined as,

$$\begin{bmatrix} I_1 \\ I_2 \\ \vdots \\ I_N \end{bmatrix} = \begin{bmatrix} Y_{11} & Y_{12} & \dots & Y_{1N} \\ Y_{21} & & & \vdots \\ \vdots & & & \vdots \\ Y_{N1} & \dots & \dots & Y_{NN} \end{bmatrix} \begin{bmatrix} V_1 \\ V_2 \\ \vdots \\ V_N \end{bmatrix} \tag{2.12}$$

The individual components can be obtained by superposition principle as,

$$Z_{ij} = \left.\frac{V_i}{I_j}\right|_{I_k=0 \text{ for } k\neq j} \tag{2.13}$$

2.4.3 Scattering Parameter

The scattering parameter matrix provides a more complete description of a network as seen from N ports. For the network described in the previous section, the scattering matrix or $[S]$ matrix is defined as

$$\begin{bmatrix} V_1^- \\ V_2^- \\ \vdots \\ V_N^- \end{bmatrix} = \begin{bmatrix} S_{11} & S_{12} & \dots & S_{1N} \\ S_{21} & & & \vdots \\ \vdots & & & \vdots \\ S_{N1} & \dots & \dots & S_{NN} \end{bmatrix} \begin{bmatrix} V_1^+ \\ V_2^+ \\ \vdots \\ V_N^+ \end{bmatrix} \tag{2.14}$$

or,

$$[V^-] = [S][V^+] \tag{2.15}$$

The elements of [S] matrix can be determined as

$$S_{ij} = \left.\frac{V_i^-}{V_j^+}\right|_{V_k^+=0 \text{ for } k\neq \text{J}} \tag{2.16}$$

2.4.3.1 Reflection Coefficient

For a two-port network, S_{11} denotes the ratio of reflected and transmitted wave in port 1 when port 2 is terminated in a matched load. This is also called the reflection coefficient.

$$S_{11} = \left.\frac{V_1^-}{V_1^+}\right|_{V_2^+=0} = \left.\frac{Z_{in}^{(1)} - Z_0}{Z_{in}^{(1)} + Z_0}\right|_{Z_0 \text{ on port } 2} \tag{2.17}$$

2.4.3.2 Transmission Coefficient

The parameter S_{21} denotes the ratio of the transmitted wave at port 2 and the incident wave at port 1, when port 2 is terminated with characteristic impedance. This parameter is also called the transmission coefficient.

$$S_{21} = \left.\frac{V_2^-}{V_1^+}\right|_{V_2^+=0} \tag{2.18}$$

2.5 Basic Hexagonal Patch Antenna

Hexagon is the basis for the hexaflake patch and thus it is beneficial to understand the radiation process of a basic hexagonal patch antenna. The freedom of xy plane gives the possibility of a number of possible shapes that can be realized by the microstrip structure, and thus hexagon can also be a possible candidate. A hexagonal patch microstrip antenna is an area of metallisation in the shape of a hexagon, that is supported above a metallic ground plane and fed with respect to the ground at an appropriate point.

The FR-4 substrate can be etched to pattern the hexagonal patch structure shown in Figure 2.5. The antenna can be fed with either a microstrip patch or a coaxial feed. For the present work only coaxial feed is considered as it is more

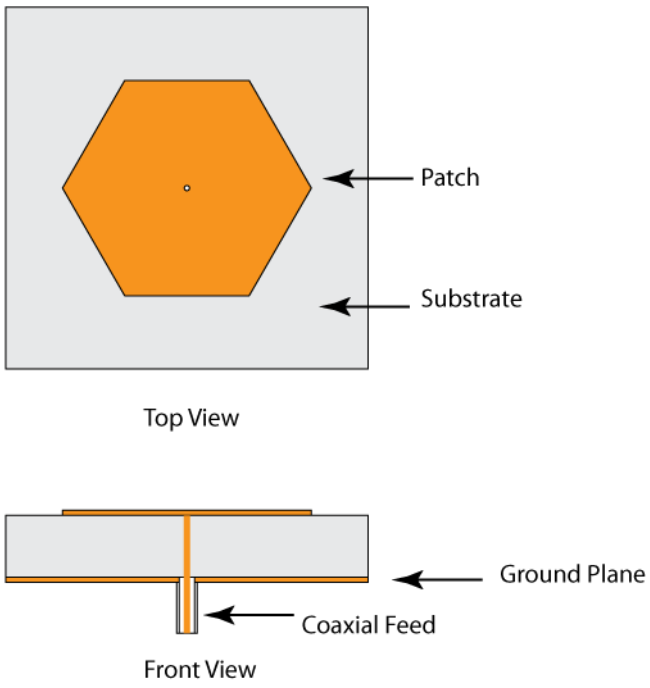

Figure 2.5: Basic Hexagonal Patch

flexible to change the feed point location. Coaxial feed has further advantage as the feed lies behind the radiating surface of the patch and therefore does not contribute to any unwanted radiation, as opposed to stripline feeds that can act as part of the antenna itself. [20]

The principle of operation of a basic patch is explained by Garg et al. [22]. A patch when connected to a microwave source would establish charge distribution on the upper and lower surfaces of the patch, and also to the surface of the ground

plane. The repulsion between same charges at the bottom suface of the patch tend to push some charges from the bottom surface around its edge to the top surface and create current densities. Since for designed patch, FR-4 substrate is very thin compared to the patch dimension ($d/W << 1$) so the tangential magnetic field produced by the vertical current flow are neglected and field variation along the height is considered to be constant. Thus the patch can be modelled as a cavity that is bounded by magnetic walls along its edge. Only TM modes are possible in this configuration.

2.5.1 Equivalent Sources of the Hexagonal Patch

Each sidewall of the cavity represent narrow apertures or slots through which radiation of EM wave occurs.
Using Huygen's field equivalence principle [18], the slots and patch metalization can be represented by equivalent electric and magnetic current densities. For thin substrate, the top electric current density is negligible compared to the bottom of the metallic patch. The electric current density ($\vec{J_s}$) and magnetic current density ($\vec{M_s}$)in the slots are given by,

$$\vec{J_s} = \hat{n} \times \vec{H_a} \tag{2.19}$$

$$\vec{M_s} = -\hat{n} \times \vec{E_a} \tag{2.20}$$

Where $\vec{H_a}$ and $\vec{E_a}$ is the slot aperture magnetic and electric field respectively. Since it is assumed that the tangential magnetic fields are negligible, the corresponding electrical current density given by Equation (2.19). The only significant source present in the patch would be the magnetic current density ($\vec{M_s}$). Again, since the ground plane is present, according to image theory, the equivalent current density would be doubled. The radiation of the patch can be thought to be as six peripheral magnetic current densities radiating in free space. So equation (2.20) can be modified as

$$\vec{M_s} = -2\hat{n} \times \vec{E_a} \tag{2.21}$$

2.6 Radiation Conductance of Hexagonal Patch

For this analysis, the hexagonal patch is assumed to be fed at the center using a coaxial probe. The coaxial probe can be modelled by the transmission line model.

The patch antenna can be modelled as radiating slots. The concept of radiating slots to explain transmission line modelling of patch antenna was first proposed by Derneryd [23]. The concept proposed by him is expanded here for hexagonal patch antennas.
The microstrip radiating element is a combination of a conducting material sheet above a ground plane separated by a dielectric material having small thickness. Derneryd explained the operation of a rectangular patch by assuming it to be equivalent to two radiating slots separated by a low impedance transmission line. When utilizing a hexagonal patch with coaxial feed, the feed acts as a point source and voltage of the feed point is distributed along the periphery of the patch. The periphery of the hexagon can be assumed to be composed of slots, formed by the opening at the dielectric medium by the upper and lower conductor cross sections.

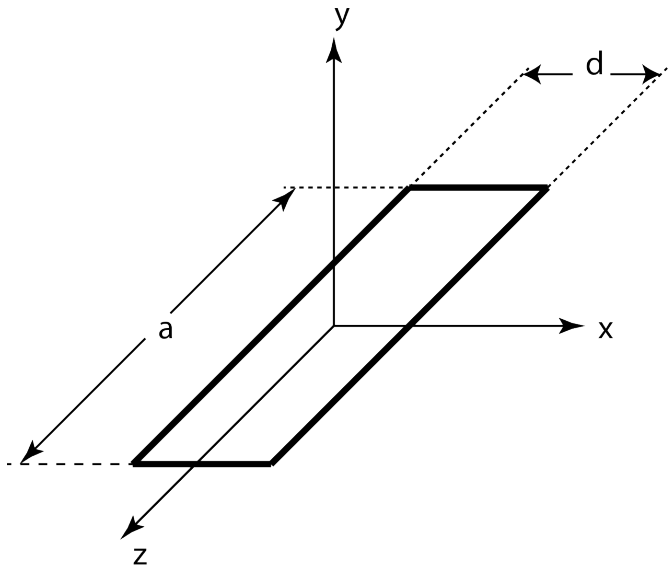

Figure 2.6: Single Slot of a Hexagonal Patch

A single slot as shown in Figure 2.6, the axes in this figure are rotated, and the x axis in Figure 2.6 actually denotes the direction of radiation in Figure 2.5. According to the assumptions stated in the previous sections, only the x directed electric field is present in the slot and the electric field is zero elsewhere.

Accordingly, the equivalent magnetic current produced by the electric field is given by Equation 2.21. Equation 2.22 gives a vector potential function .

$$\mathbf{F}(\mathbf{r}) = \varepsilon_0 \int_c \frac{\mathbf{M}(\mathbf{r})}{4\pi \left|\mathbf{r} - \mathbf{r}'\right|} e^{-jk_0|\mathbf{r}-\mathbf{r}'|} dl(\mathbf{r}') \tag{2.22}$$

For the slot, the potential function can be obtained by, [23]

$$F_z = \frac{e^{-jk_0 r}}{4\pi r} 2E_x ad \frac{\sin\left(\frac{k_0 h}{2}\sin\theta\cos\phi\right)\sin\left(\frac{k_0 a}{2}\cos\theta\right)}{\frac{k_0 h}{2}\sin\theta\cos\phi\frac{k_0 a}{2}\cos\theta} \tag{2.23}$$

The far field electric field can be written as,

$$E_\phi = -jk_0 F_z \sin\theta \tag{2.24}$$

Let, the voltage across the slot, $V_0 = dE_x$. If the substrate thickness is small, $k_0 d << 1$, Equation 2.24 can be written as,

$$E_\phi = -j\frac{V_0}{\pi}\frac{e^{-jk_0 r}}{r}\frac{\sin\left(\frac{\pi a}{\lambda_0}\cos\theta\right)}{\cos\theta}\sin\theta \tag{2.25}$$

where $\lambda_0 = \frac{2\pi}{k_0}$ is the free space wave length.

The power can be written as,

$$P = \int_v \nabla \cdot \mathbf{E} \times \mathbf{H}^* dv \tag{2.26}$$

using value of E_ϕ from Equation 2.25, the value of P is found to be,

$$P = \frac{1}{2}\sqrt{\frac{\epsilon}{\mu}}\frac{V_0^2}{\pi}\int_0^\pi \frac{\sin^2\left(\frac{\pi a}{\lambda_0}\cos\theta\right)}{\cos^2\theta}\sin^3\theta d\theta \tag{2.27}$$

For a single slot, the voltage across the slot is V_0 . So the power can be approximated as a power dissipated through an equivalent conductance.

$$P = \frac{1}{2}\frac{V_0^2}{R_r} = \frac{1}{2}V_0^2 G$$

Where G is the radiation conductance.

The value of G can thus be written as,

$$G = \frac{1}{\pi}\sqrt{\frac{\epsilon}{\mu}}\int_0^\pi \frac{\sin^2\left(\frac{\pi a}{\lambda_0}\cos\theta\right)}{\cos^2\theta}\sin^3\theta d\theta \tag{2.28}$$

The value of G can be obtained by numerically evaluating the integration of Equation 2.28. For small value of width, if $a/\lambda_0 << 1$, the integration can be approximated by the following formula. [23]

$$G = \frac{1}{90}\left(\frac{a}{\lambda_0}\right)^2 \tag{2.29}$$

and if the value of a is larger and tends to infinity, then G can be approximated with,

$$G = \frac{1}{120}\left(\frac{a}{\lambda_0}\right) \tag{2.30}$$

Since the hexagonal patch is composed of 6 slots, ignoring their mutual coupling, the slot conductance of each of the slots can be obtained from Equation 2.28.

2.7 Conclusion

In this chapter, various aspects of antenna parameters and also fundamental concepts of microstrip antenna was discussed. The concepts of Impedance and Scattering Parameters are introduced. Some analysis methods of patch antenna such as Transmission Line Model, Cavity Model and Finite Element Method were discussed. Furthermore, Basic structure of the hexagonal patch is discussed, and the radiation mechanism for the hexagonal patch element is discussed. The determination of radiation conductance for one side of a hexagonal patch element is discussed here. The value of radiation conductance is used in the next chapter for multiport modelling.

Chapter 3

Multiport Analysis of Hexagonal Patch

3.1 Introduction

Multiport Network Approach to solve problems regarding arbitrary shaped patch has been described by Gupta [24]. Basically an arbitrary shaped patch is assumed to consist of several elementary shaped patch for which the Green's function is known. And Z-matrix characterisation is determined from the Green's function. The modelling of radiating patches and fringing field are incorporated by addition of appropriate Edge Admittance Network (EAN).

3.2 Mathematical Derivation

3.2.1 Segmentation Method

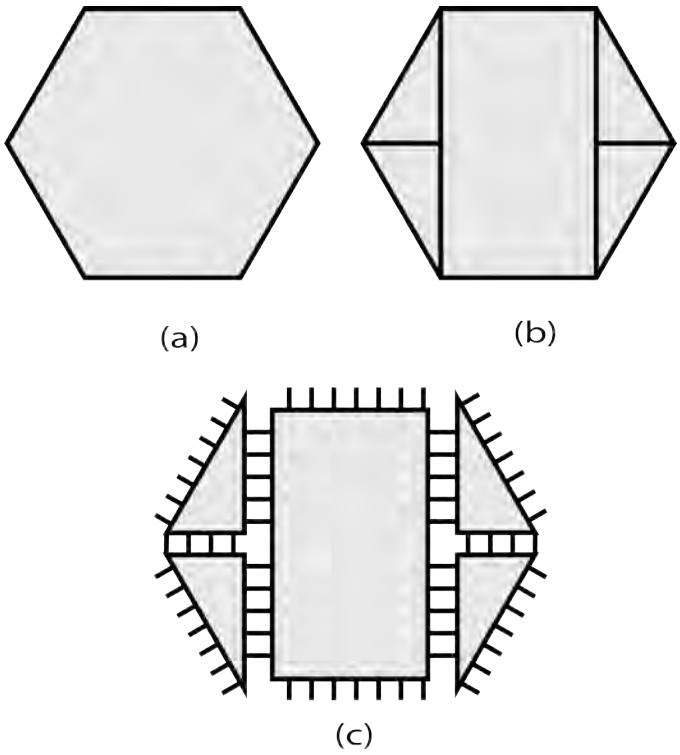

Figure 3.1: (a) Basic Hexagonal Structure (b) Structure divided into triangles and rectangle (c) Multiport Representation of a hexagonal patch

For a shape for which the Green's function is defined as the doubly infinite summation with terms corresponding to various modes of planar resonance with magnetic wall, the Z matrix characterization can be written as,

$$Z_{ij} = \frac{1}{W_i W_j} \int_{W_i} \int_{W_j} G(x_i, y_i | x_j, y_j) ds_i ds_j \tag{3.1}$$

In equation 3.1 where x_{ij} , y_{ij} denote the location of two ports of width W_i and W_j respectively.

A basic hexagonal structure can be divided into a rectangle and four right angled $30° - 60°$ triangle.

3.2.2 Z-matrix for basic rectangular and triangular segments

The Green's function for rectangular patch is given by,

$$G(x_i, y_i|x_j, y_j) = \frac{j\omega\mu d}{ab} \sum_{n=0}^{\infty} \sum_{m=0}^{\infty} \frac{\sigma_m \sigma_n cos(k_y y_0) cos(k_x x_0) cos(k_x x) cos(k_y y)}{k_x^2 + k_y^2 - k^2} \tag{3.2}$$

Where,

$$\begin{aligned} k_x &= \frac{m\pi}{a} \\ k_y &= \frac{n\pi}{b} \\ k^2 &= \omega^2 \mu \epsilon_0 \epsilon_r (1 - j\delta) \\ \sigma_i &= \begin{cases} 1, i = 0 \\ 2, i \neq 0 \end{cases} \end{aligned} \tag{3.3}$$

Green's function for right angled $30° - 60°$ triangle can be written as

$$G(x_i, y_i|x_j, y_j) = 8j\omega\mu d \sum_{n=0}^{\infty} \sum_{m=0}^{\infty} \frac{T_l(x_0, y_0) T_l(x, y)}{16\sqrt{3}\pi^2(m^2 + mn + n^2) - 9\sqrt{3}a^2k^2} \tag{3.4}$$

Where,

$$\begin{aligned} T_l(x, y) = (-1)^l cos\left(\frac{2\pi l x}{\sqrt{3}a}\right) cos\left[\frac{2\pi(m-n)y}{3a}\right] \\ +(-1)^m cos\left(\frac{2\pi m x}{\sqrt{3}a}\right) cos\left[\frac{2\pi(n-l)y}{3a}\right] \\ +(-1)^n cos\left(\frac{2\pi n x}{\sqrt{3}a}\right) cos\left[\frac{2\pi(l-m)y}{3a}\right] \end{aligned} \tag{3.5}$$

By substituting value of Green's function into Equation 3.1 the Z-matrix components can be computed. For rectangular patch, for two ports p and q located at (x_p, y_p) and (x_q, y_q) the components of Z-matrix can be obtained by the equation

suggested by Benalla et al. [25],

$$Z_{pq} = \frac{j\omega\mu d}{ab} \sum_{m=0}^{\infty} \sum_{n=0}^{\infty} \frac{\sigma_m \sigma_n \phi_{mn}(x_p, y_p) \phi_{mn}(x_q, y_q)}{k_x^2 + k_y^2 - k^2} \tag{3.6}$$

For ports oriented along y direction, the value of $\phi_{mn}(x, y)$ is given by,

$$\phi_{mn}(x, y) = cos(k_x x) cos(k_y y) sinc\left(\frac{k_y w}{2}\right) \tag{3.7}$$

and for ports oriented along x direction

$$\phi_{mn}(x, y) = cos(k_x x) cos(k_y y) sinc\left(\frac{k_y w}{2}\right) \tag{3.8}$$

Faster computation of above parameters are possible by reducing the double integral to single integral [25]. If port p and q are oriented along the same direction, the Z parameter for port p and q can be obtained by,

$$\begin{aligned} Z_{pq} = -CF\frac{1}{\eta}\left[\sum_{l=0}^{L} \frac{\sigma_l cos(k_u u_p) cos(k_u u_q) cos(\gamma_l z_>) cos(\gamma_l z_<) sinc\left(\frac{k_u w_p}{2}\right) sinc\left(\frac{k_u w_p}{2}\right)}{\gamma_l sin(\gamma_l F)}\right] \\ -jCF\frac{1}{\eta}\left[\sum_{l=L+1}^{\infty} \frac{cos(k_u u_p) cos(k_u u_q) sinc\left(\frac{k_u w_p}{2}\right) sinc\left(\frac{k_u w_p}{2}\right) e^{-j\gamma_l (v_> - v_<)}}{\gamma_l}\right] \end{aligned} \tag{3.9}$$

where, condition is set that if both ports p and q are oriented along y direction, $l = m$ condition is set, and if both ports are located along x direction, $l = n$ is chosen.

For ports p and q oriented along different direction, (x and y) the Z parameter matrix elements can be obtained by,

$$\begin{aligned} Z_{pq} = -CF\frac{1}{\eta}\left[\sum_{l=0}^{L} \frac{\sigma_l cos(k_u u_p) cos(k_u u_q) cos(\gamma_l z_>) cos(\gamma_l z_<) sinc\left(\frac{k_u w_p}{2}\right) sinc\left(\frac{\gamma_l w_q}{2}\right)}{\gamma_l sin(\gamma_l F)}\right] \\ -jCF\frac{1}{\eta}\left[\sum_{l=L+1}^{\infty} \frac{cos(k_u u_p) cos(k_u u_q) sinc\left(\frac{k_u w_p}{2}\right) e^{-j\gamma_l (v_> - v_< - w_q/2)}}{\gamma_l^2 w_q}\right] \end{aligned} \tag{3.10}$$

The summation bound l is chosen so that the summation is converged, and thus

$$\begin{aligned} l = m, \ \text{if} \ y_> - y_< - w_{j/2} > 0 \\ l = n, \ \text{if} \ x_> - x_< - w_{j/2} > 0 \end{aligned} \tag{3.11}$$

and if both the condition are satisfied, any choice of $l = m$ or $l = n$ would result in convergence.

The different parameter values can be obtained by,

$$F = \begin{cases} b, \ \text{if} \ l = m \\ a, \ \text{if} \ l = n \end{cases}$$

$$(u_p, u_q) = \begin{cases} (x_p, x_q), \ \text{if} \ l = m \\ (y_p, y_q), \ \text{if} \ l = n \end{cases}$$

$$\gamma_l = \pm\sqrt{k^2 - k_u^2}$$

$$k_u = \begin{cases} \frac{m\pi}{a}, \ \text{if} \ l = m \\ \frac{n\pi}{b}, \ \text{if} \ l = n \end{cases}$$

$$(z_>, z_<) = \begin{cases} (y_> - b, y_<), \ \text{if} \ l = m \\ (x_> - a, x_<), \ \text{if} \ l = n \end{cases}$$

According to Lee [26], right angled $30° - 60°$ triangle the Z matrix can be computed as,

$$Z_{pq} = 8j\omega\mu h \sum_{m=-\infty}^{\infty} \sum_{n=-\infty}^{\infty} \frac{I_{T_l}(p) I_{T_l}(q)}{16\sqrt{3}\pi^2(m^2 + mn + n^2) - 9\sqrt{3}a^2k^2} \tag{3.12}$$

where $l + m + n = 1$ and a is the length of hypotenuse of the triagle, and I_{T_l} takes different values depending on the location of port p along the sides of the triangle.

- When port p is located along the side opposite to the 30° side,

$$I_{T_l}(p) = H^1(l, x_p, w_p) + H^1(m, x_p, w_p) + H^1(n, x_p, w_p) \tag{3.13}$$

- When port p is located along the side opposite to the 60° side,

$$I_{T_l}(p) = H^2(m-n, y_p, w_p) + H^2(n-l, y_p, w_p) + H^2(l-m, y_p, w_p) \tag{3.14}$$

- When port p is located along the side opposite to the 90° side,

$$I_{T_l}(p) = H^2(2(m-n), y_p, w_p/2) + H^2(2(n-l), y_p, w_p/2) + H^2(2(l-m), y_p, w_p/2) \tag{3.15}$$

Where functions H^1 and H^2 is given by,

$$H^1(k,t,w) = (-1)^k cos\left(\frac{2\pi k}{\sqrt{3}a}t\right) \times sinc\left(\frac{2\pi k}{\sqrt{3}a}\frac{w}{2}\right) \tag{3.16}$$

$$H^2(k,t,w) = (-1)^k cos\left(\frac{2\pi k}{3a}t\right) \times sinc\left(\frac{2\pi k}{3a}\frac{w}{2}\right) \tag{3.17}$$

The above equations were employed to calculate individual Z parameter matrix for a basic rectangular segment and 30-60-90 triangle.

3.2.3 Segment joining to form Z-Parameter matrix of an unloaded hexagonal patch

The Figure 3.2 a shows the segmentation of hexagon into part A, B, C, D, E where A, B, D, E are identical 30°-60°-90° triangles, for which Z parameter matrix can be calculated using Equation (3.12). Considering only part A and B, the two parts have some ports which are joined together, and some other ports that are unconnected and connected to other segments. For simplicity, firstly only segment A and B is considered to be joined. Segment A has external ports $\mathbf{P_A}$ and ports that are connected to B segment denoted by $\mathbf{q}$. Similarly, segment B also has $\mathbf{P_B}$ ports and ports connected to A denoted by $\mathbf{r}$. The Z matrix of each of the segments A and B can be written in terms of sub matrices as

$$\mathbf{Z_A} = \begin{bmatrix} \mathbf{Z_{p_a}} & \mathbf{Z_{p_a q}} \\ \mathbf{Z_{q p_a}} & \mathbf{Z_{qq}} \end{bmatrix}, \mathbf{Z_B} = \begin{bmatrix} \mathbf{Z_{p_b}} & \mathbf{Z_{p_b r}} \\ \mathbf{Z_{r p_b}} & \mathbf{Z_{rr}} \end{bmatrix} \tag{3.18}$$

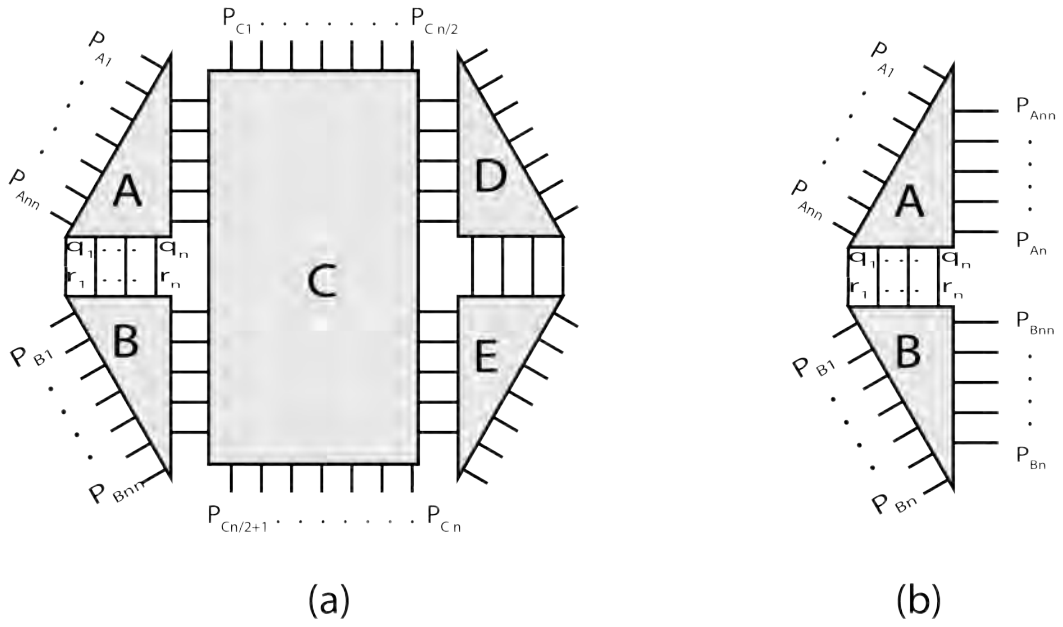

Figure 3.2: (a) Segmentation of unloaded hexagonal patch into part A, B, C, D, E(b) Joining part A and B

Combining these two arrays give,

$$\mathbf{Z_{AB}} = \begin{bmatrix} \mathbf{Z_{p_a}} & 0 \\ 0 & \mathbf{Z_{p_b}} \end{bmatrix} + \begin{bmatrix} \mathbf{Z_{p_a q}} \\ -\mathbf{Z_{p_b r}} \end{bmatrix} [\mathbf{Z_{qq}} + \mathbf{Z_{rr}}] \begin{bmatrix} -\mathbf{Z_{qp_a}} & \mathbf{Z_{rp_b}} \end{bmatrix} \tag{3.19}$$

The combined AB segment is identical if the segment DE is joined, and thus $\mathbf{Z_{AB}} = \mathbf{Z_{DE}}$. The port sequence of DE segment is arranged appropriately as it is attached to the opposite side of the Basic Rectangular Patch. Equation (3.19) can be used to compute the parameters of the pentagonal shape formed by joining segment AB and C showed in Figure 3.2.

3.2.4 Modeling Radiation of Hexagonal Patch

The patch shown in Figure 3.2 is unloaded. To find out the radiation characteristics of the patch, it has to be loaded. Figure 3.3 shows a Edge Admittance Network (EAN) for a typical radiating edge of a patch antenna. [22]

The edge admittance network conductance corresponds to the loading, occurs due to the radiation from the patch antenna, and the capacitance corresponds to the fringing electric field.

Loading the network shown in Figure 3.2 with the edge admittance network shown in Figure 3.3 enables to model the radiation of the patch. The coaxial feed

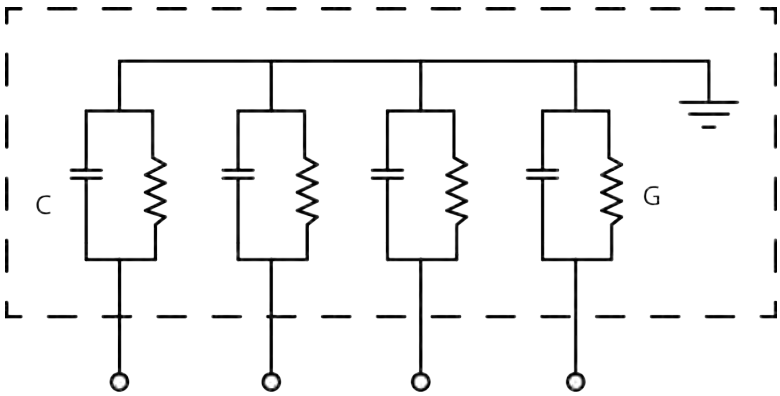

Figure 3.3: Edge Admittance Network

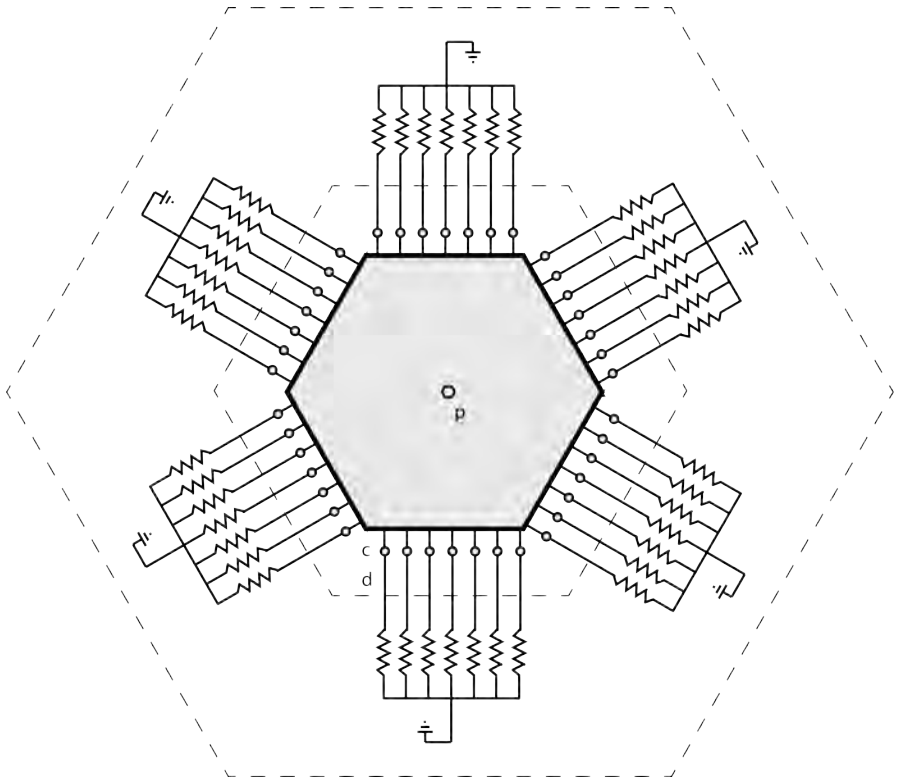

Figure 3.4: Loaded Hexagonal Patch Multiport Model

of the antenna is represented with equivalent planar feed. The complete multiport model of the loaded antenna is shown in Figure 3.4 . The entire radiation resistance network can be treated as a seperate multiport network, connected to the unloaded hexagonal patch model. Ports corresponding to the patch and the EAN network are represented by c_i and d_i respectively. The equivalent radiation resistance can be calculated using Equation 2.28 for one side of the hexagonal patch element. The conductance G is then divided into all the ports parallel to one side of the hexagon.

The current input into the side of the patch to some ports are then transmitted through the Z parameter network into the other ports and through the Radiating Edge Admittance network. If a current I_P is fed into the pth port of the antenna, which corresponds to the coaxial feed, this current is modelled with an equivalent current fed into a port on the periphery of the patch. The Z matrix parameters for the different segments shown in Figure 3.4 can then be written as,

$$\begin{bmatrix} \mathbf{V}_p \\ \mathbf{V}_c \\ \mathbf{V}_d \end{bmatrix} = \begin{bmatrix} \tilde{Z}_{pp} & \tilde{Z}_{pc} & \tilde{Z}_{pd} \\ \tilde{Z}_{cp} & \tilde{Z}_{cc} & \tilde{Z}_{cd} \\ \tilde{Z}_{dp} & \tilde{Z}_{dc} & \tilde{Z}_{dd} \end{bmatrix} \begin{bmatrix} \mathbf{I}_p \\ \mathbf{I}_c \\ \mathbf{I}_d \end{bmatrix} \tag{3.20}$$

Here p represent the feed ports, c and d represent the interconnected ports shown in Figure 3.4. For a current fed in port p, the voltages at the c and d ports are given by,

$$\mathbf{V_c} = \mathbf{V_d} = [\tilde{Z}_{cp} + [\tilde{Z}_{cc} - \tilde{Z}_{cd}][\tilde{Z}_{cc} + \tilde{Z}_{dd}]^{-1}[\tilde{Z}_{dp} - \tilde{Z}_{cp}]]\mathbf{I_p} \tag{3.21}$$

Equation 3.21 can be used to calculate the voltage around the radiating edge of the patch. This voltage can be used to calculate the electric field E_z around the periphery.

E_z can be represented by an equivalent magnetic current, $\mathbf{M}$. Thus the electric vector potential at a distance $\mathbf{r}$ can be represented by Equation 2.22,

This equation can be written in discrete form as,

$$F(\mathbf{r}) = \varepsilon_0 \sum_{1}^{n} \frac{M_i}{4\pi \left|\mathbf{r} - \mathbf{r'}_i\right|} e^{-jk_0|\mathbf{r}-\mathbf{r'}_i|} \tag{3.22}$$

As the currents in each port connected to the radiation resistances are known by applying ohms law to the voltages obtained from Equation 3.21, the currents M_i are obtained. The far field at distance $\mathbf{r}$ is then obtained from the components

of $\mathbf{F}(\mathbf{r})$ as

$$E_\theta = \eta H_\phi = jk_0 F_\phi = jk_0(-F_x sin\phi + F_y cos\phi) \tag{3.23}$$

$$E_\phi = \eta H_\theta = jk_0 F_\theta = jk_0(-F_x cos\phi + F_y sin\phi)cos\theta \tag{3.24}$$

3.3 Multiport Analysis of a Hexagonal Patch

The method discussed in the previous section was used to model a hexagonal patch element to study its properties. MATLAB was used to compute the Z parameter of the multiport model. The obtained Z matrix for the hexagonal patch element becomes ill-conditioned, and thus it becomes difficult to compute the far field radiation pattern without loss of computational accuracy.

3.4 Conclusion

In this chapter, a different theoretical treatment was attempted for the hexagonal patch to better understand its radiation properties. The method is easier to comprehend for the different geometrical structure of the hexagonal patch compared to the cavity model, but it is more computationally feasible to analyse the antenna using Finite Element Method.

Chapter 4

Simulation of Hexagonal Patch

4.1 Introduction

The hexagonal patch structure mentioned in the previous chapters has been simulated. In this chapter, the simulation method and the results of simulation for the hexagonal patch has been discussed. The simulation setup is repeated for the iteration of hexaflake structures.

4.1.1 Antenna Substrate

The basic hexagonal patch structure was simulated using Ansoft HFSS software. The metallic patch is modelled using Perfect Electric Conductors and the FR-4 substrate is taken as per the material library of the software. FR-4 is an industry standard for Printed Circuit Board (PCB) fabrication substrate, and thus the design of the antenna could be easily fabricated using printed circuit technology. The properties of FR-4 is shown in Table 4.1.

Table 4.1: Properties of FR-4 Substrate

Property	Value
Relative Permittivity, ϵ_r	4.47
Loss Tangent, δ	0.01646
Thickness, d	1.57×10^{-3} m

4.2 Modelling of Coaxial Feed

The coaxial feed is modelled with a perfectly conducting cylinder bounded by insulator and PEC boundary. The model is shown in the Figure 4.1. The radius of the inside conductor of the coaxial cable is 0.7mm and the outer conductor diameter is 2.3 mm.

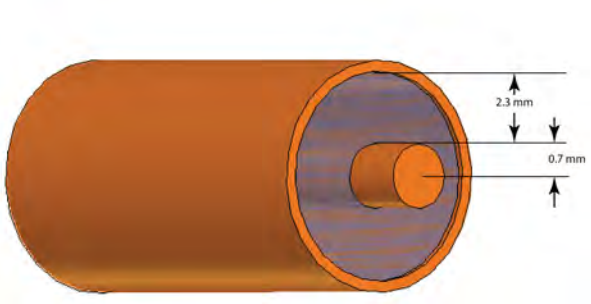

Figure 4.1: Coaxial Feed Model

4.2.1 Resonance for different patch size

Figure 4.2 shows the simulation model of the patch. Simulation software used was Ansoft HFSS simulation software.

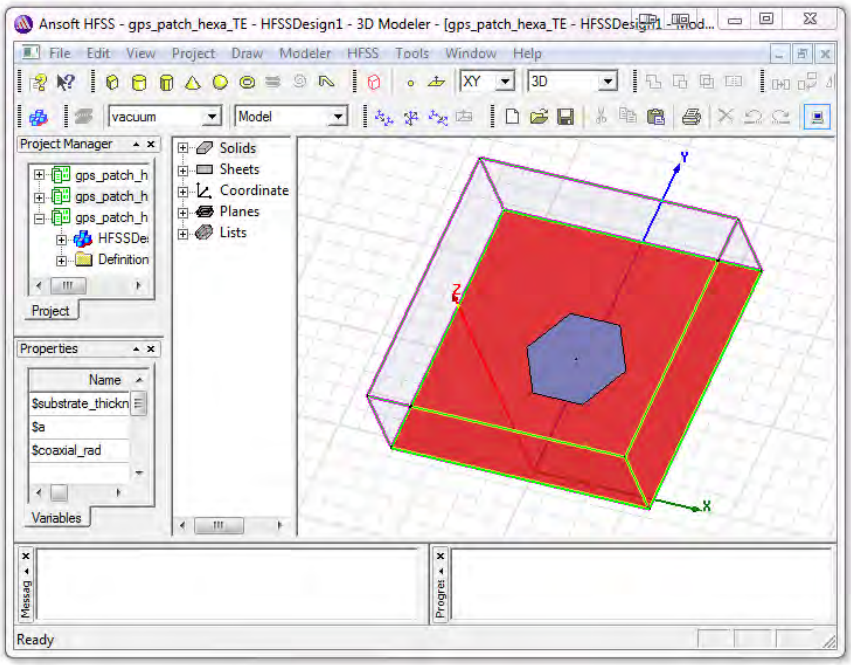

Figure 4.2: Simulation of Basic Hexagonal Patch

In order to find out the resonance condition of the patch, the side of the hexagon, a is varied and for different values of a, the reflection coefficient S_{11} is obtained. The result for parametric sweep is shown in Figure 4.3.

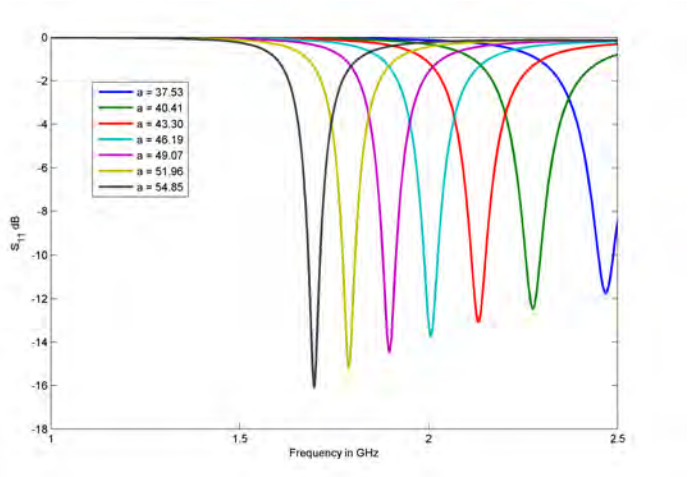

Figure 4.3: Return loss of basic hexagonal patch at different values of a

4.2.1.1 Center Frequency at different values of sidelength, a

It can be seen from Figure 4.3 that the resonance occurs at a particular frequency where the reflection coefficient (S_{11}) at the input port decreases rapidly. For antenna operation, the value of S_{11} in dB should be less than -10. So the frequency band between which the value stays below -10 gives an operating band.

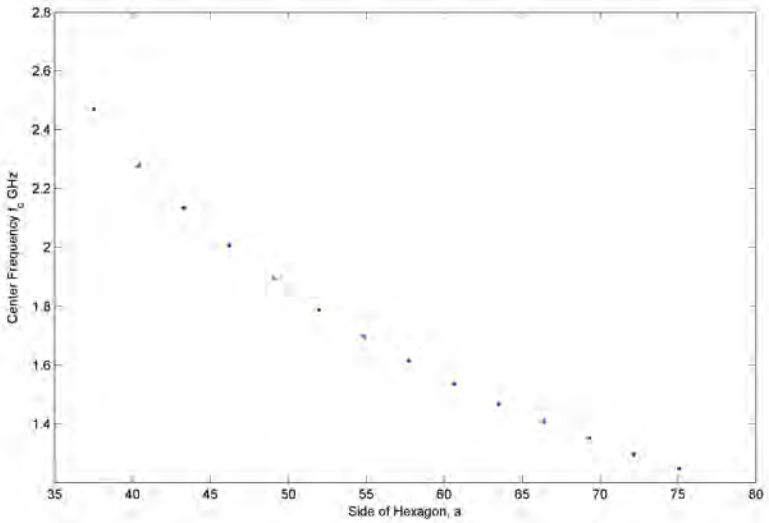

Figure 4.4: Center Frequency of First Band of basic hexagonal patch at different values of a

Center frequency of the first band of operation for the basic hexagonal patch decreases as the value of a increases. This is expected as the value of larger patch size implies smaller resonance frequency as the increased dimension of the patch results in larger value of capacitance as per transmission line model. The change of center frequency vs a is illustrated in Figure 4.4. The change of center frequency with respect to the side length can be modelled by curve fitting as,

$$f_c = -(2.1658 \times 10^{-6})x^3 + 8.2253 \times 10^{-4})x^2 - 0.11503x + 7.0548 \tag{4.1}$$

4.2.1.2 Bandwidth at different values of sidelength, a

Figure 3.4 shows the bandwidth of the basic hexagonal patch antenna for different values of a.

Here the value of bandwidth used can be written as:

$$BW = \frac{f_2 - f_1}{f_c} \times 100\% \tag{4.2}$$

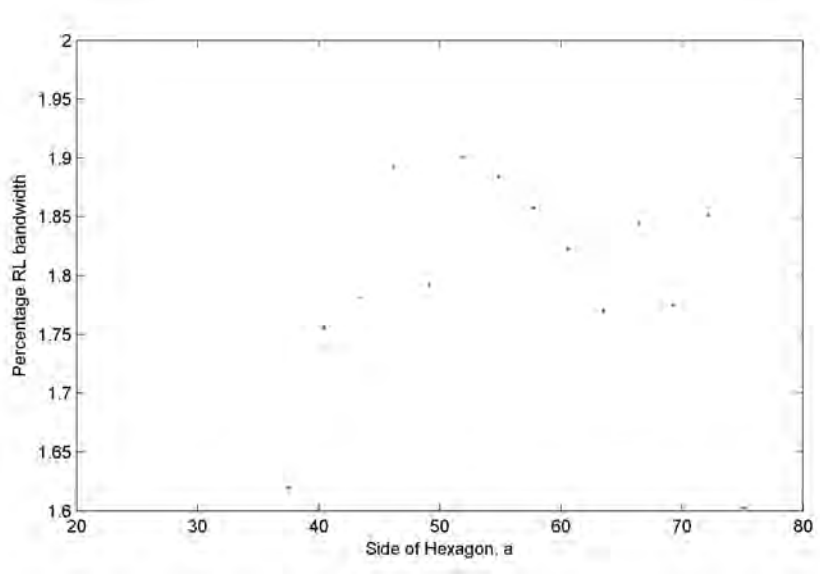

Figure 4.5: Return Loss Bandwidth of First Band of basic hexagonal patch at different values of a

Where f_2 and f_1 are the The percentage bandwidth for the basic hexagonal patch is around 1.8%. It can also be seen that the bandwidth is not strongly dependent on the value of a

4.2.2 Comparison with simulation results of a rectangular patch

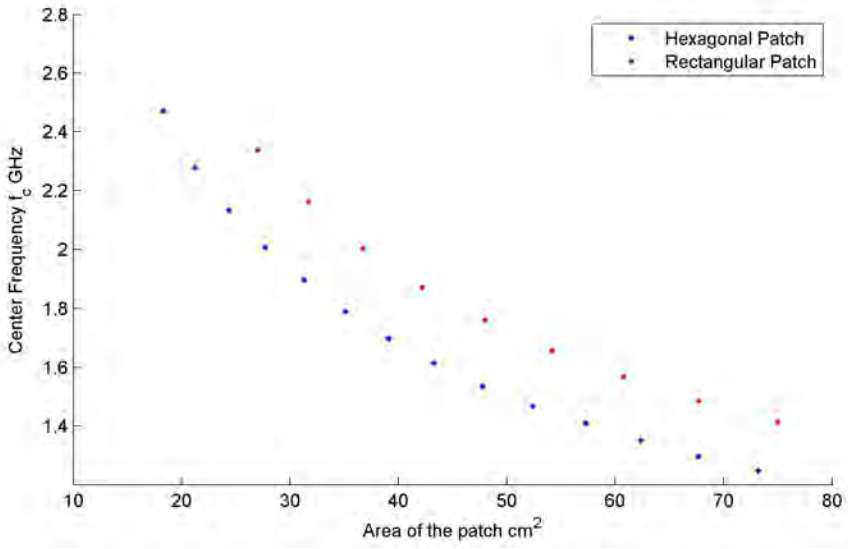

Figure 4.6: Center Frequency of first band vs basic hexagonal patch and rectangular patch at different values of a

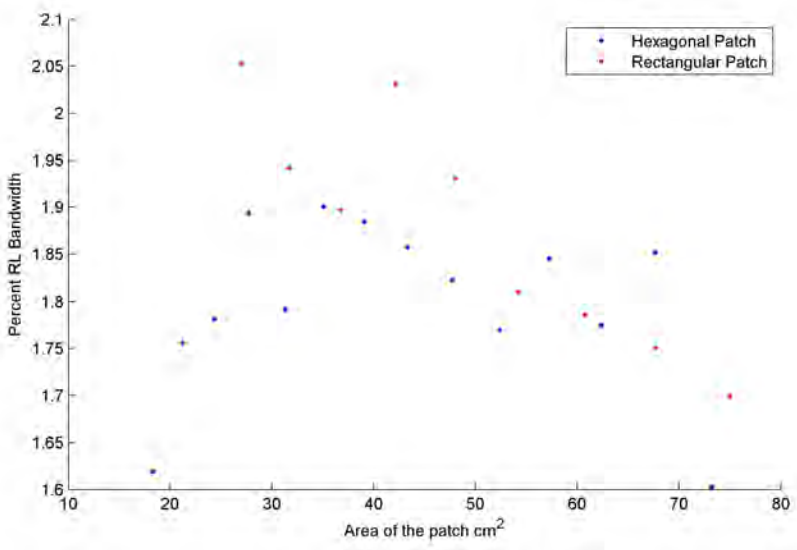

Figure 4.7: RL Bandwidth of first band vs basic hexagonal patch and rectangular patch at different values of a

The simulation results are compared to an equivalent size rectangular patch antenna. The patch area in mm^2 is taken and for different patch areas the center frequency of first band and return loss bandwidth is measured. The center frequency of the rectangular patch and hexagonal patch element is shown in Figure 4.6. From the figure it can be seen that the center frequency of a hexagonal patch element is lower compared to the center frequency of a rectangular patch element at the same patch area. This means that for same patch area, a hexagonal patch structure can reduce the center frequency compared to a rectangular patch structure. The RL bandwidth of rectangular and hexagonal patch at different patch areas is shown in Figure 4.7. It can be seen that the bandwidth of hexagonal patch is comparable to the rectangular patch structure.

4.3 Conclusion

The simulation of hexagonal patch structure shows improvement in the patch area over the traditional rectangular patch. Thus it is further interesting to know if the iteration of the hexagonal patch into hexaflake structures yield performance improvement.

Chapter 5

First Iteration of Hexaflake Patch

5.1 Introduction

In this chapter, the first iteration of hexaflake fractal is studied as a patch structure. In the previous chapter hexagonal patch element is shown to have size reduction compared to rectangular patch element. The hexaflake fractal iteration is shown first, and afterwards, the effect of increasing coupling width, patch size and changing feed position is studied.

5.2 Patch Structure

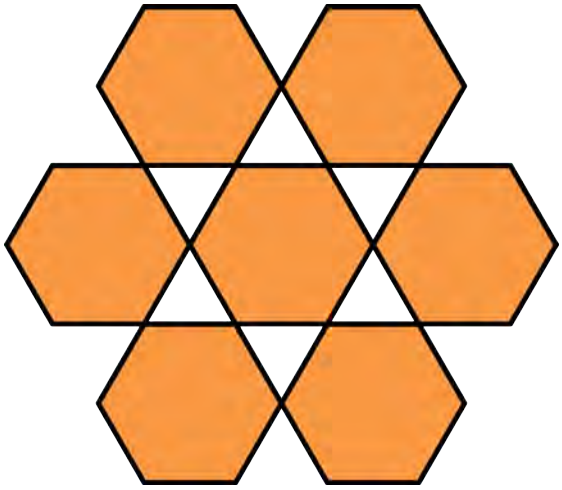

Figure 5.1: First Iteration of Hexaflake Structure

To make a iteration of a basic hexagon to hexaflake structure, if the side of the hexagon is of a length, 7 smaller hexagons each having side length of $a/3$ are taken, and arranged in the manner shown in Figure 5.1. The smaller hexagons in a perfect hexaflake structure are connected in a single point only, and this small point of contact is difficult to maintain in manufacturing process and also the small segment means higher resistance between different parts of the patch. Accordingly, it was observed if the contact width of the patch can be increased to yield better performance of the antenna. The contact width are termed to be coupling width.

5.3 Effect of Changing Coupling Width

The coupling width between the different elements of the fractal are changed to give better conductivity within the patch. Figure 5.2 shows the structure of coupling between the adjacent elements. The coupling is made scaling invariant of patch by assuming the width of the coupling to be a/cs, where cs is the coupling scaling

factor. Higher value of cs means smaller width of coupling segment, thus the antenna would act more like a pure hexaflake fractal, but it would also result in lower conductivity, where higher value of cs means wider coupling between elements.

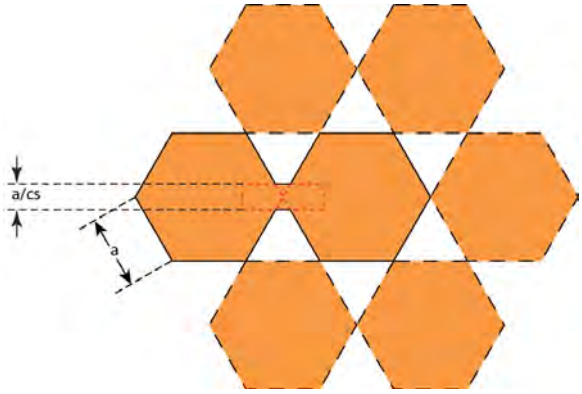

Figure 5.2: Coupling width with scaling factor cs

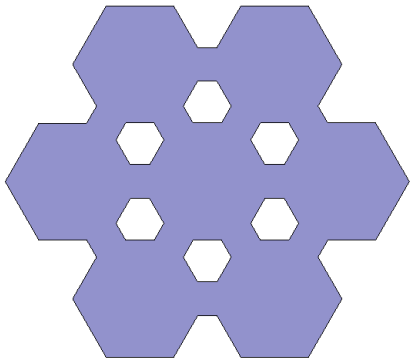

Figure 5.3: Iteration of Fractal Structure with $cs = 4$

To find out the effect of changing the value of cs on the bandwidth, FEM analysis was performed on the first iteration of the hexaflake. The effect of varying cs on return loss is shown on Figure 5.4 (a=70mm). The bandwidth of the antenna decreases rapidly as the value of cs is decreased. But also, it reduces the center frequency of the hexagonal patch antenna.

The effect on the shift of center frequency on the port width is shown in Figure 5.5. Comparing result with $a = 70$ found in the Figure 4.3, it can be seen that the first hexaflake not only dramatically reduces the center frequency of the antenna, but also gives rise to a lower band of operation.

The simulation results show that the value of $a/4$ is required feed width for successful operation as a patch antenna of the first iteration fractal. Accordingly, the value of $a/4$ is used for successive simulations of the patch.

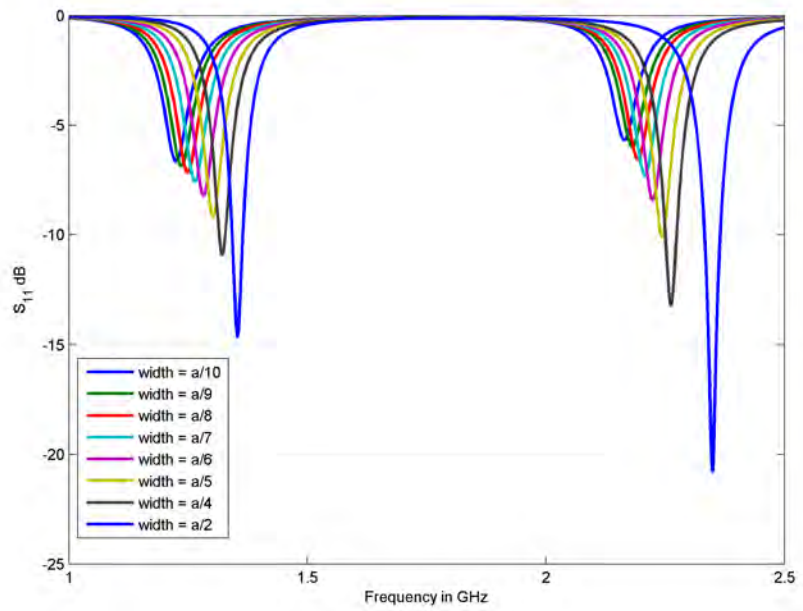

Figure 5.4: Return loss for varying coupling width

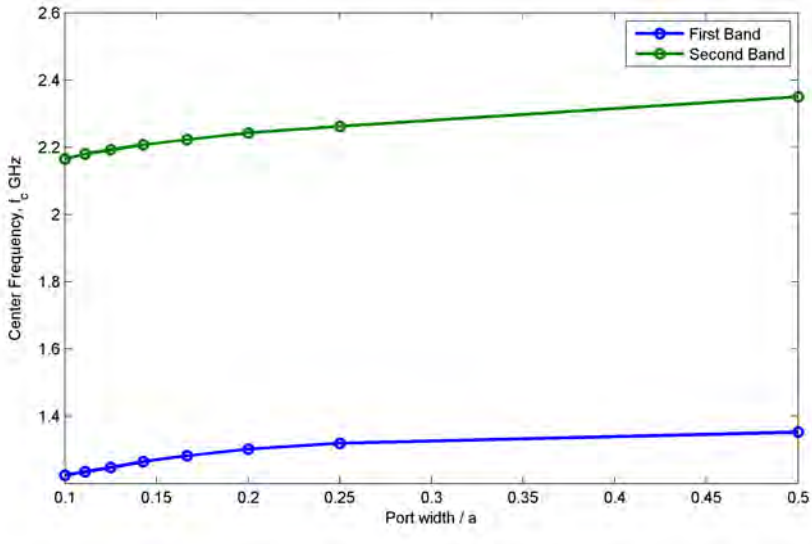

Figure 5.5: Change of center frequency for varying individual port lengths

5.4 Varying the Side Length of Center-fed First Iteration of Hexaflake

If the side length of the hexaflake is changed, it is expected that the center frequency will change as the basic hexagonal fractal structure. All basic patch strucures reduce the resonant frequency as the patch size is is increased.

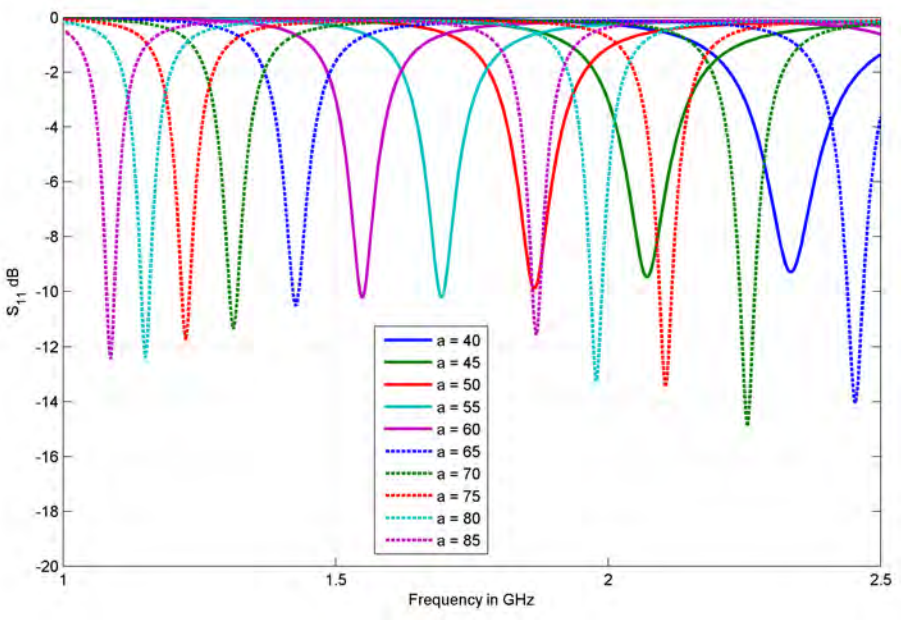

Figure 5.6: Return loss of first iteration of hexaflake structre patch with variation of patch size

Figure 5.6 shows the return loss of the first iteration of hexaflake patch. As expected the increased value of a which result in larger patch area decreases the center frequency. As the coupling width has been made scaling invariant by choosing the width as $a/4$, smaller size patch also results in smaller coupling between the elements. This is evident as the return loss bandwidth of the antenn is reduced as the patch size is reduced. To optimally operate the patch antenna, for smaller size patch, the coupling width need to be further increased, while in larger patch, the coupling width can be decreased to match a specific return loss bandwidth specification.

Figure 5.7 shows the variation of center frequency as the patch size is changed for the first iteration of hexaflake fractal structure. It is evident that the the center frequency rapidly increases as the patch size is decreased for both the operating frequency bands.

The change of frequency can be modelled with the following curve fitting equations:

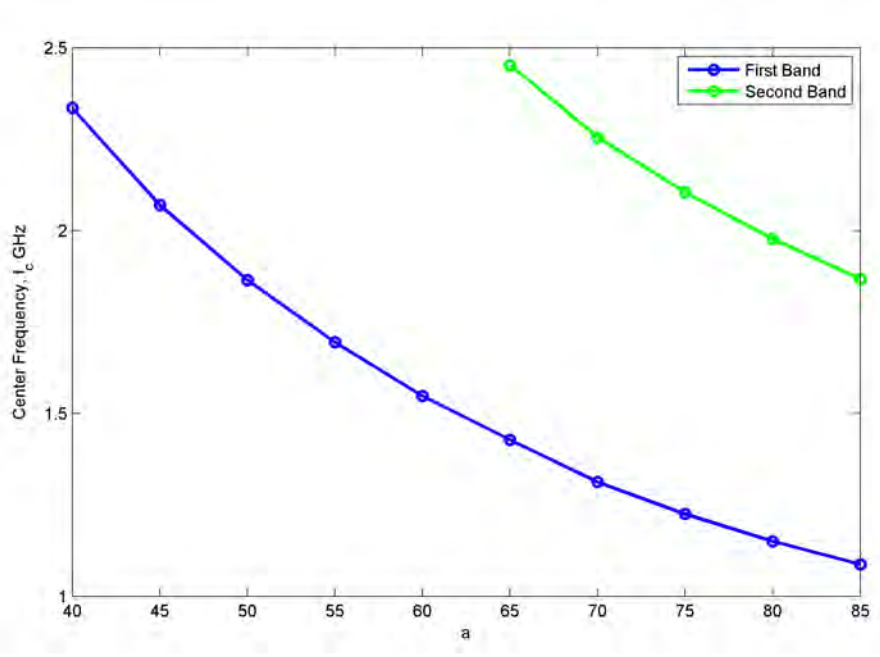

Figure 5.7: Center frequency of first iteration of hexaflake patch structure with variation of patch size

$$f_{c_1} = -(5.9324 \times 10^{-6})a^3 + (1.5612 \times 10^{-3})a^2 - (0.15029)a + 6.2217 \tag{5.1}$$

$$f_{c_2} = -(2 \times 10^{-6})a^3 + (5.0643 \times 10^{-3})a^2 - (50643)a + 15.759 \tag{5.2}$$

Where f_{c_1} and f_{c_2} is the center frequency of the first and second band respectively, given in GHz, and a is given in mm.

5.5 Optimum Feed Position

In this section the effect of changing the feed position for the the fractal antenna from the center position is studied. Since the first iteration hexaflake patch structure is symmetric in x and y direction, the effect of changing the feed position along the x axis is observed.

Figure 5.8 shows the variation of feed position along the x axis of the patch antenna. The feed position is changed by a scaling invariant positioning. 8 possible feed position are studied, where feed position is $\frac{na}{9}$. The value of $n = 0$ represents the center fed position. The value of $n = 3$ represents the feed point to be located on the coupling element. The value of $n = 6$ represent the feed is on the center of

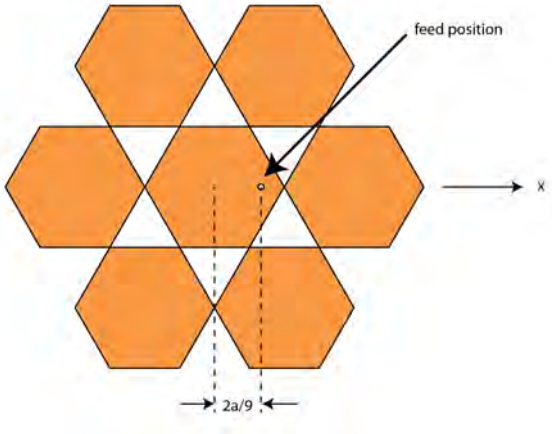

Figure 5.8: Variation of feed position of the first iteration of hexaflake patch

a smaller hexagon on the periphery of the fractal structure.

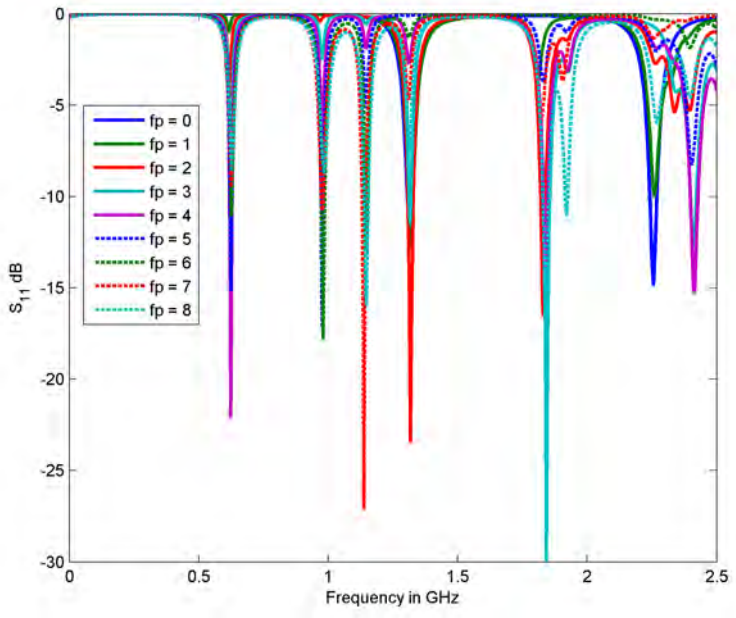

Figure 5.9: Return loss for Varying feed position of the first iteration of hexaflake patch

Figure 5.9 shows the return loss for the various feed positions of the first iteration of the hexaflake patch antenna. The return loss largely varies on the feed position. For antenna operation, the return loss should be below -10dB and accordingly the operating bands are found from the values of S_{11}.

Table 5.1 shows the resulting frequency bands for varying feed position of the first iteration of hexaflake fractal patch antenna. Only if the return loss attained a

Table 5.1: First iteration hexaflake fractal patch antenna center frequency and RL Bandwidth

Feed Point	First Band		Second Band		Third Band		Fourth Band	
	fc (GHz)	%BW	fc (GHz)	%BW	fc (GHz)	%BW	fc (GHz)	%BW
0	1.3125	1.1429	2.2563	1.2188	-	-	-	-
1	1.3188	1.3270	2.2613	0.1106	-	-	-	-
2	1.3188	1.7062	1.8313	1.2287	1.7850	1.9608	2.3538	1.8056
3	0.6250	0.8000	1.3175	0.7590	1.8438	1.4915	2.4113	0.9331
4	0.6250	1.6000	1.8413	0.9504	2.4150	1.2422	2.4000	2.5000
5	0.6250	1.6000	0.9775	1.0230	2.3863	1.7810	-	-
6	0.6275	0.7968	0.9813	1.2739	1.1488	0.6529	-	-
7	0.9788	0.7663	1.1400	1.3158	-	-	-	-
8	1.1475	1.3072	1.8413	1.2220	1.9200	0.5208	-	-

value below -10dB, the operating range is regarded as a frequency band. From the table it can be seen that if the position of the feed is $x = \frac{3a}{9}$ or $x = \frac{4a}{9}$ it yields an operating band, and also the resonant frequency (f_c) is reduced compared to the first iteration of hexaflake fractal. For $a = 70mm$, both position yields the first center frequency as 0.55 GHz, so the patch size can be further reduced to attain same resonant frequency.

5.6 Effect of Substrate Thickness

It has been reported [18] that increased substrate thickness tend to increase the bandwidth of the antenna. Since the proposed antenna structure is to be fabricated using printed circuit technology, the thickness can be increased by adding multiple layers of PCB copper board etched from copper and adding a ground plane.

Figure 5.10 shows the configuration of increasing substrate thickness of the patch antenna by adding additional layers of dielectric FR4 sheets. The structure was simulated for different positions of the feed. The resulting return loss is shown in Figure 5.11. The return loss of the antenna differ significantly as the feed position is changed, while the operating frequencies remain same. Since the antenna operation requires return los below -10 dB, only the bands that meet this criteria are selected as operating bands. Table 5.2 shows the center frequency and percentage return loss bandwidth for the operating bands of for the increased thickness.

By comparing data from Table 5.1 and 5.2 it can be seen that for feed position 3 and for value of $a = 70mm$, the bandwidth is changed. The increased thickness also causes the return loss in different frequencies to change due to change in the fringing fields. To compare the results, the lowest frequency band which existed

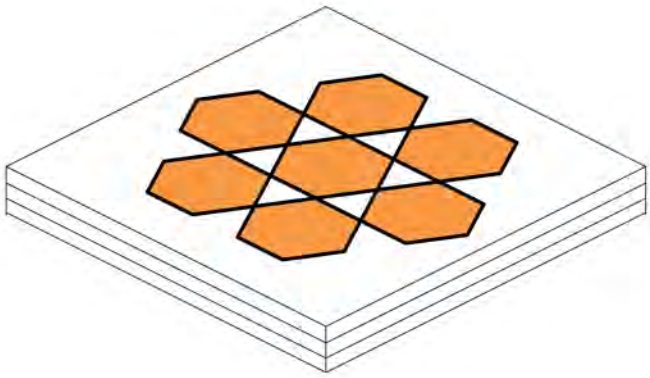

Figure 5.10: Increasing Layer thickness for first iteration hexaflake

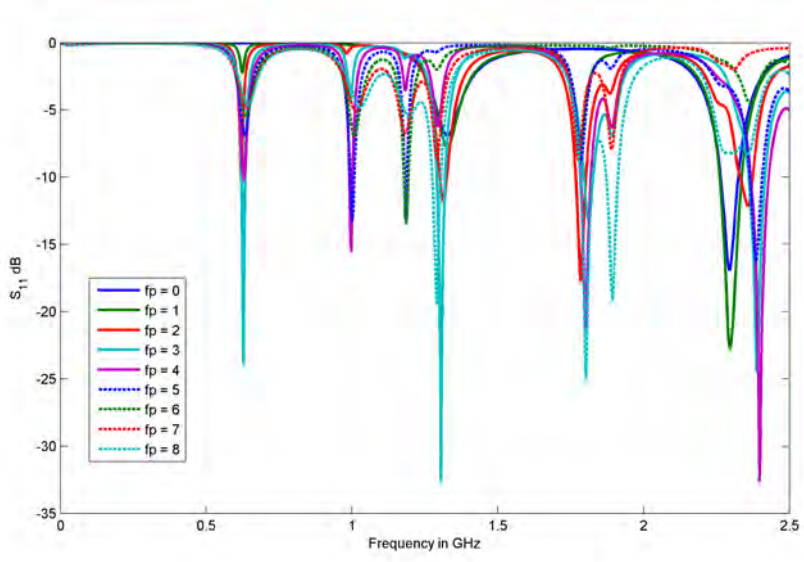

Figure 5.11: Return loss for triple substrate thickness for first iteration hexaflake

Table 5.2: Increased substrate thickness first iteration hexaflake center frequency and RL Bandwidth

Feed Point	First Band		Second Band		Third Band		Fourth Band	
	fc (GHz)	%BW	fc (GHz)	%BW	fc (GHz)	%BW	fc (GHz)	%BW
0	2.295	2.614	-	-	-	-	-	-
1	2.300	3.261	-	-	-	-	-	-
2	0.621	0.402	1.315	1.901	1.785	1.961	2.354	1.806
3	0.629	1.988	1.308	2.294	1.814	1.792	2.390	2.301
4	0.630	0.794	0.998	1.003	1.803	1.942	2.400	2.500
5	1.003	1.496	1.185	0.844	2.386	1.781	-	-
6	1.188	1.263	-	-	-	-	-	-
7	-	-	-	-	-	-	-	-
8	1.291	2.130	1.805	2.216	1.893	2.114	-	-

for both the normal FR-4 substrate and the three layer substrate are taken. The bands which didn't exist in any of the two cases are discarded.

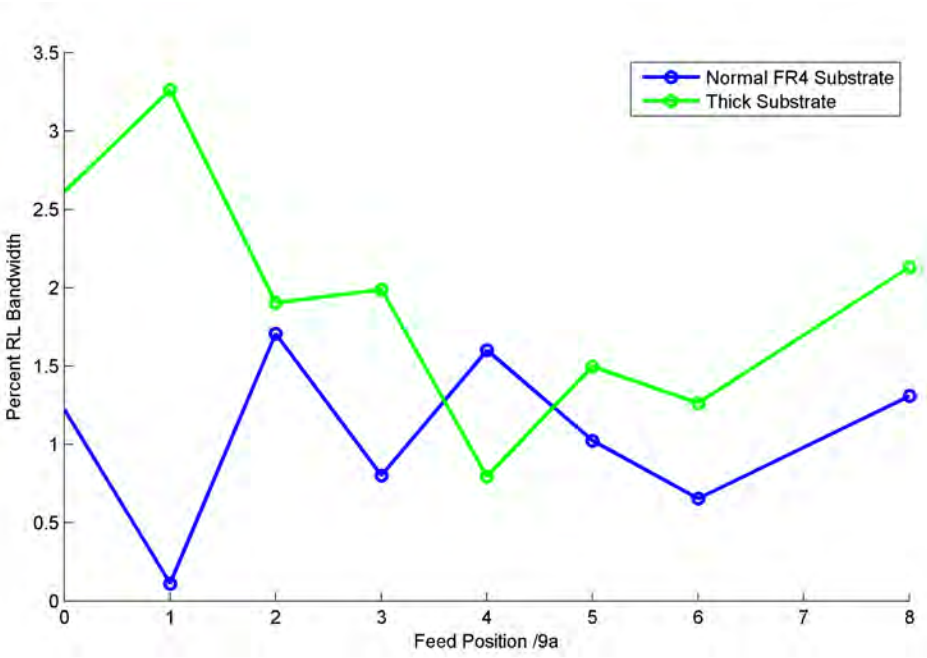

Figure 5.12: Change of RL Bandwidth with substrate thickness

Figure 5.12 shows the percentage BW in the bands that exist in both normal and thick substrates. It can be seen that in most cases the bandwidth can be increased by increasing the substrate thickness. For that matter thicker non-standard variant of FR-4 should be fabricated which is a more difficult process.

5.7 Conclusion

In this chapter the first iteration of hexaflake fractal structure is studied. The effect of changing fractal dimension, coupling width and optimum feed position of the fractal has been studied.

Chapter 6

Second Iteration of Hexaflake Patch

6.1 Introduction

In this chapter, the second iteration of hexaflake fractal structure is explored as a possible patch antenna structure. The first iteration of hexaflake fractal showed considerable amount of patch size reduction, thus it is beneficial to know whether the further iteration of fractal augments the improvement of the antenna.

6.2 Patch Structure

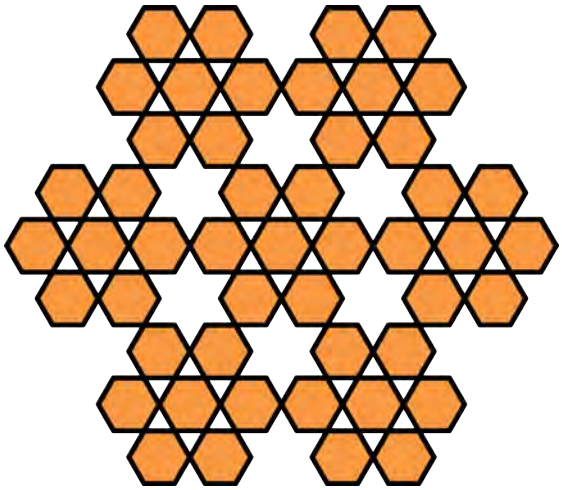

Figure 6.1: Second Iteration of Hexaflake Structure

The structure shown in Figure 5.1 can be repeated in a similar manner to generate the second iteration. To make a iteration of the first iteration of hexaflake, 7 smaller structures of the first iteration are taken with each having side length of $(a/3)/3$, where $a/3$ was the side length of the first iteration. They are arranged in the manner shown in Figure 6.1. Similar to the first hexaflake structure, the smaller hexagons in a perfect hexaflake structure are connected in a single point only, and this small point of contact is difficult to maintain in manufacturing process and also the small segment means higher resistance between different parts of the patch. Accordingly, it was observed if the contact width of the patch can be increased to yield better performance of the second fractal structure.

6.3 Effect of Changing Coupling Width

The contact width between the different elements of the fractal are changed to give better conductivity within the patch structure. As with the Figure 5.2, the coupling between adjacent elements of the patch are enhanced by increasing the

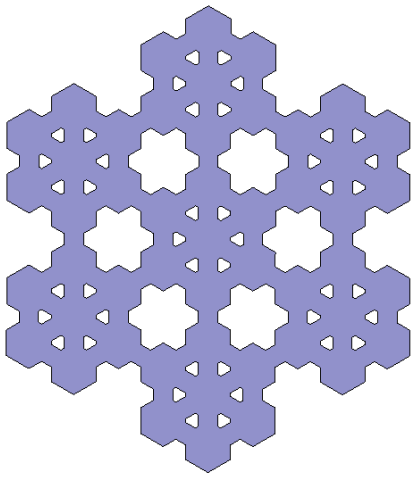

Figure 6.2: Second Iteration of Hexaflake Structure with extended port width

width of the hexagon at the end. The coupling is made scaling invariant by making the width of the coupled port as $a/cs/3$ port width of the fractal. As the smaller segments of the second iteration has a side length of $a/9$, the coupling width needs to be scaled with the factor of $1/3$.

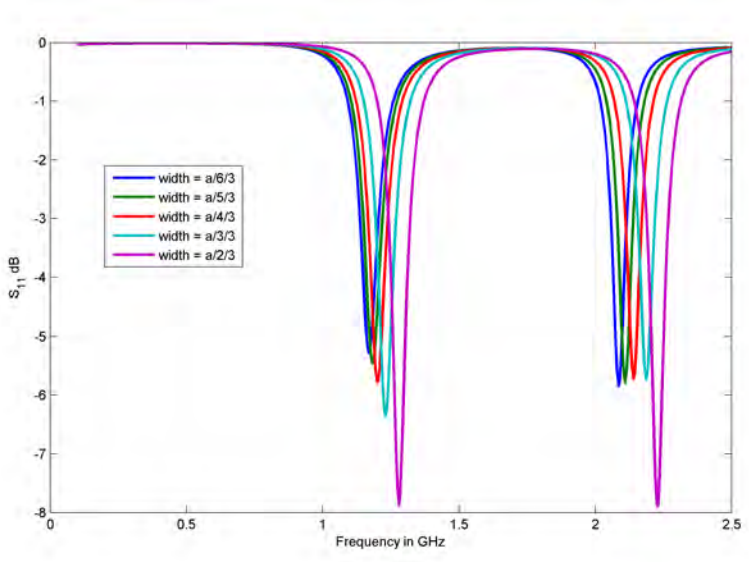

Figure 6.3: Return loss of Second Iteration Hexaflake by varying coupling width

Figure 6.2 shows a hexaflake fractal structure that has a coupling width of $a/4/3$. The coupling width are smaller compared to the first fractal structure and therefore gives rise to conductivity problem within the patch.

Figure 6.3 shows the return loss for various coupling width at a second iteration hexaflake patch.

The second iteration has smaller basic hexagonal elements that make up the patch and accordingly, the coupling between the patches are too small to provide adequete conductance to the adjacent fractal elements.

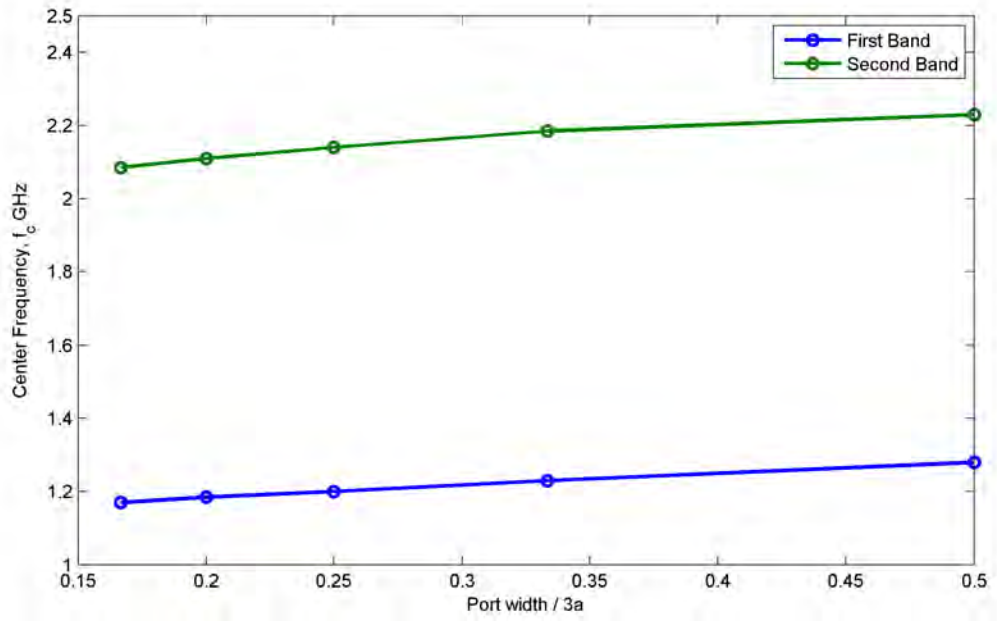

Figure 6.4: Varying coupling width of Second Iteration Hexaflake

Accordingly, in the figure, the return loss of the second fractal at $a = 70mm$ stays above $-10dB$ even though the coupling width is maximally increased without distorting the fractal structure. So the second iteration of hexaflake structure cannot appreciably work as a fractal antenna structure at $a = 70mm$. It would be beneficial to check if the fractal can work in center frequencies. The center frequency variation of the second iteration is shown in Figure 6.4. It can be seen that the center frequency of the resonant patch is reduced as the coupling width between elements is reduced. Comparing the results with Figure 5.5, it is observed that the second iteration of hexaflake fractal further reduces the center frequency of the patch.

6.4 Optimal Feed Position

The previous sections discussed the effect of feeding the fractal antenna in the center position. It is useful to know whether changing the feed position can yield better performance for the antenna. Since the second iteration hexaflake patch

structure is self-symmetric in x and y direction, the effect of changing the feed position along the x axis is observed. As the element size are further reduced here, only feed positions at the center of the smaller elements and feed is observed, and further positional variation on each smaller element is ignored.

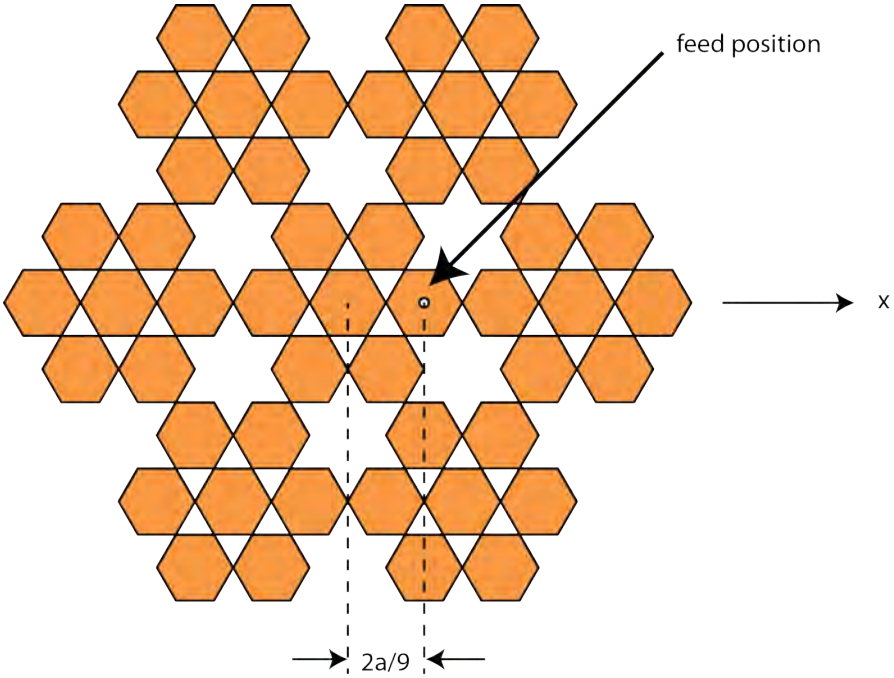

Figure 6.5: Varying feed position of the second iteration of hexaflake patch

Figure 6.5 shows the variation of feed position along the x axis of the patch antenna. The feed position is changed by a scaling invariant positioning. Eight possible feed position are studied, where feed position is $\frac{na}{9}$, when the value of n is even, the feed is located in the center of a smaller hexagonal element, where n odd represents that the feed is located on the coupling element between two hexagons.

Figure 6.6 shows the return loss for the various feed positions of the second iteration of the hexaflake patch antenna. The return loss largely varies on the feed position. For antenna operation, the return loss should be below -10dB and accordingly the results are studied to find the operating bands.

Table 6.1 shows the resulting frequency bands for varying feed position of the fractal. Only if the return loss attained a value below -10dB, the operating range is regarded as a frequency band.

From the table it can be seen that if the position of the feed is $x = \frac{3a}{9}$ or $x = \frac{4a}{9}$ it yields an operating band, and also the resonant frequency (f_c) is reduced compared to the first iteration of hexaflake fractal. For $a = 70mm$, both position yields the first center frequency as 0.55 GHz, so the patch size can be further reduced to

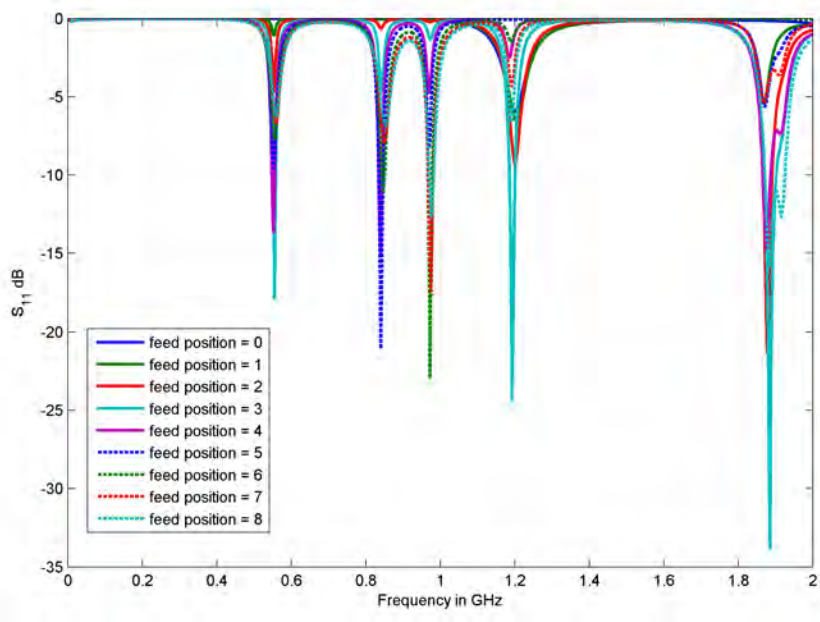

Figure 6.6: Return loss for varying feed position of the second iteration of hexaflake patch

Table 6.1: Frequency Bands obtained by varying feed position in second iteration of hexaflake

Feed Point	First Band		Second Band		Third Band	
	fc (GHz)	%BW	fc (GHz)	%BW	fc (GHz)	%BW
0	-	-	-	-	-	-
1	-	-	-	-	-	-
2	1.88	1.329787	-	-	-	-
3	0.55625	1.348315	1.195	1.25523	1.88625	1.722995
4	0.55375	1.354402	0.84125	0.89153	1.8775	1.065246
5	0.84125	1.485884	-	-	-	-
6	0.84875	0.883652	0.97375	1.283697	-	-
7	0.97625	1.28041	-	-	-	-
8	0.9775	1.023018	1.9	2.894737	-	-

attain same resonant frequency.

6.5 Varying Patch Size

To study the effect of variation of patch dimension on the antenna performance, the patch size was varied for adjusted position of feed and coupling width for which maximum bandwidth was obtained previously.

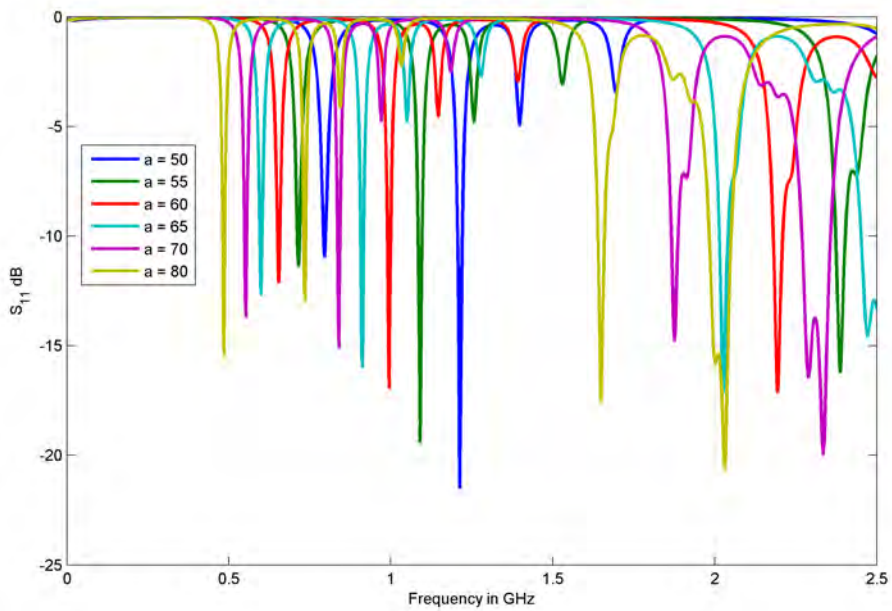

Figure 6.7: Return loss for varying fractal size of the second iteration of hexaflake patch

Figure 6.7 shows the return loss for the various patch sizes of second iteration of the hexaflake patch. As before, the reduced patch dimension increases the center frequency.

Figure 6.8 shows the center frequencies of the adjusted second iteration of the hexaflake patch. The center frequency change can be approximated by using the following curve fitting equations:

$$f_{c_1} = (-2.6087 \times 10^{-6})a^3 + (6.9203 \times 10^{-4})a^2 - (0.066631)a + 2.722 \qquad (6.1)$$

$$f_{c_2} = -(3.6957 \times 10^{-006})a^3 + (9.9803 \times 10^{-4})a^2 - (0.097964)a + 4.0766 \qquad (6.2)$$

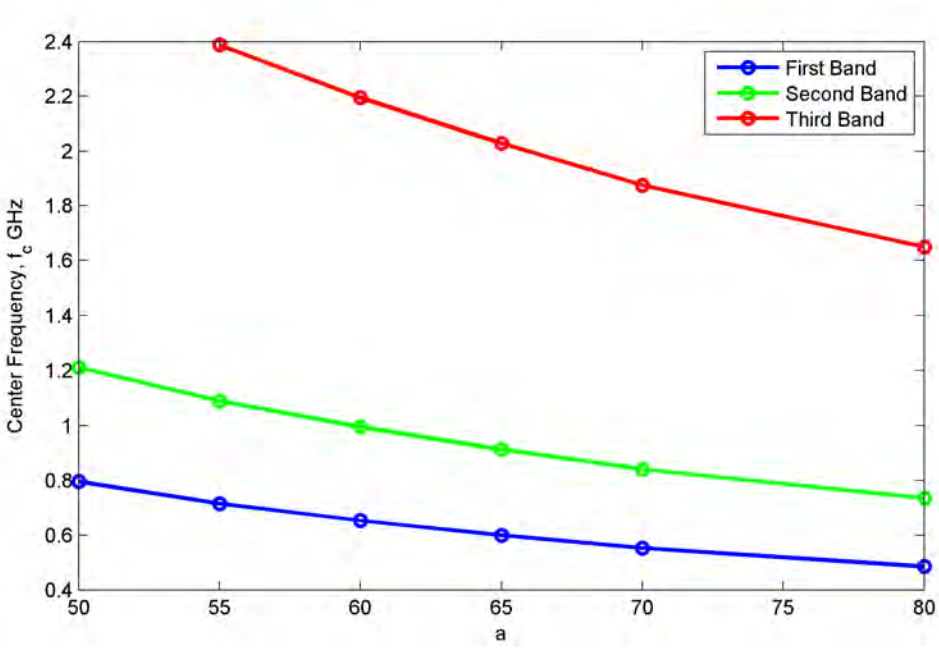

Figure 6.8: Center Frequencies of the operating bands of the second iteration of hexaflake patch

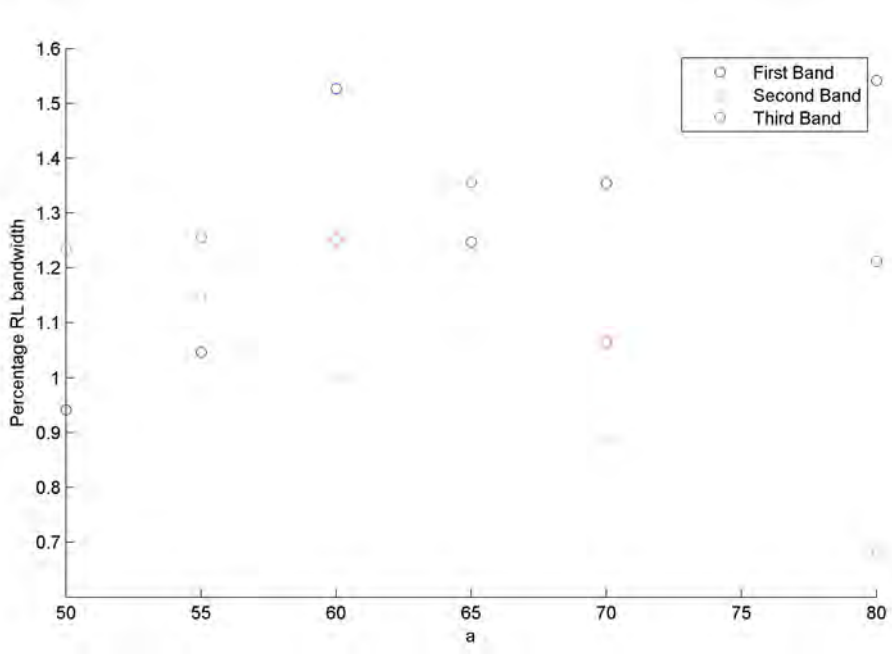

Figure 6.9: Percent RL Bandwidth of the operating bands of the second iteration of hexaflake patch

$$f_{c_3} = (2.7044 \times 10^{-006})a^3 + (9.5957 \times 10^{-5})a^2 - (0.053922)a + 5.1931 \qquad (6.3)$$

Where f_{c_1}, f_{c_2} and f_{c_3} are the center frequency of the first, second and third band respectively, given in GHz, and a is given in mm.

Figure 6.9 shows the percentage RL bandwidth for the operating bands of second iteration of the hexaflake fractal structure. From the figure it can be seen that the operating bandwidth of the second iteration of hexaflake fractal antenna is about 1%.

6.6 Conclusion

In this chapter the second iteration of hexaflake fractal structure is studied. The effect of changing fractal dimension, coupling width and optimum feed position of the fractal has been studied. The second iteration of hexaflake fractal result in tri-band operation in the studied frequency range. And the patch size is reduced compared to the basic hexagonal and first and second iteration of hexaflake patch.

Chapter 7

Effect of FSS Ground Plane

7.1 Introduction

In this chapter, the effect of adding a Frequency Selective Surface (FSS) ground plane on first iteration of hexaflake patch structure is explored.

7.2 Frequency Selective Surface

The concept of Frequency Selective Surface is to provide variable opacity for different values of the wavelength of incident radiation. FSS structures are commonly used in making reflector antenna more efficient [27], as well as to make highly directive resonator antenna [28].

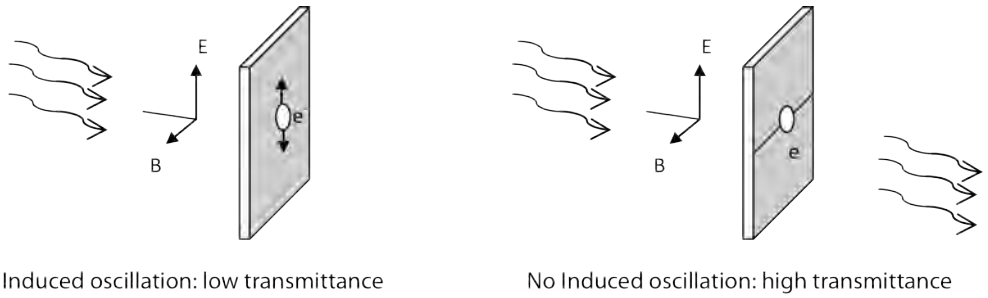

Figure 7.1: Basic Principle of Frequency Selective Surface

Figure 7.1 shows the basic operating principle of a FSS structure. If a plane wave is incident orthogonally on a metal plate that has a single electron, it would cause the electron to interact with the wave and oscillate. As the electron oscillates, it absorbs the wave energy and if all the energy is absorbed, the wave transmitted through the plane would be zero. If the motion of the electron is restricted on a wire, the wave would be absorbed only if the electron can accelerate in the direction of the electric field.

As the accelerated charge radiates according to Maxwell's principle, the electrons on the surface of the plane would radiate on both sides of the surface. These waves cause interference with the incident wave. The radiated field intensities depend on the incident wave frequency and the structure of the wire. If large portion of the incident wave is reradiated toward the incident wave, the transmittance is poor, and major portion of the wave is reflected towards the incident field. Different types of structures have been studied as elements that can selectively transmit or reflect a frequency band [29]. The four legged loaded element is a structure that exhibit a band pass property.

Figure 7.2 shows the principle of four legged loaded element. Figure 7.2 (a) represents a capacitive element, that act as a high pass filter. Low frequency waves

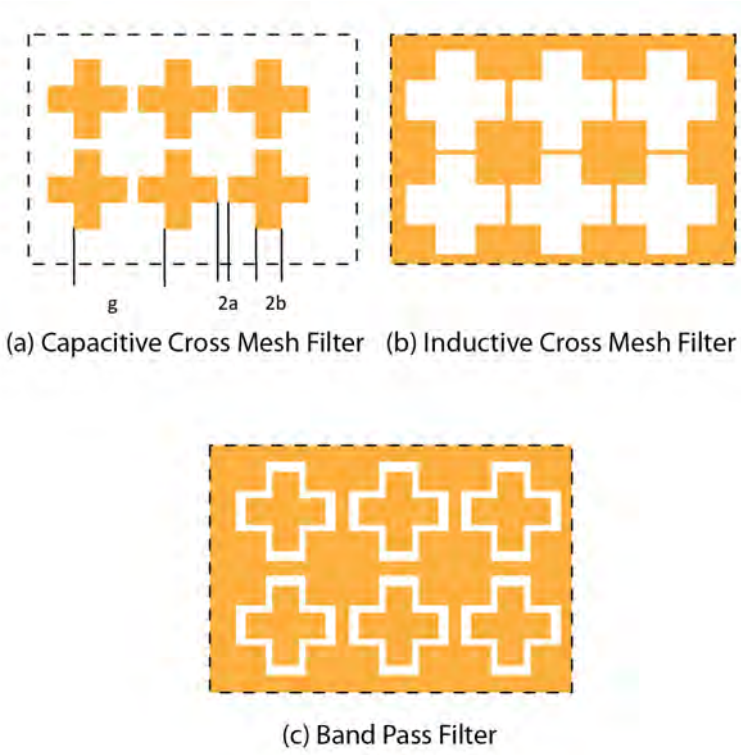

Figure 7.2: Four Legged Loaded Element as FSS

are blocked by the element, where high frequency waves can pass. Figure 7.2 (b) is the complementary structure of Figure 7.2 (a). According to the Babinet's principle, the complementary structure would exhibit opposite reflection properties of the original structure, so Figure 7.2 (b) acts as an inductive element where low frequency waves can pass, and high frequency waves are blocked. Combination of Figure 7.2 (a) and Figure 7.2 (b) yields Figure 7.2 (c), which act as a band pass filter. Typically, these elements are also fabricated using printed circuit technology on a dielectric substrate, and configured as array of elements. Choudhury et al. [30] proposed the technique of gradual circumferential variation for controlling the bandwidth of four-legged loaded element FSS structures.

Since the loaded element filter act as a band pass filter that reflect a portion of the frequency band, and also since the cavity is only formed by reflection from the frequency selective surface, it can be applied to control the bandwidth of a patch antenna. Here, only the application to hexaflake patch antenna is done to find out the effect on the application of FSS ground plane.

7.3 Array of Four legged loaded element

To illustrate the possibility of using a FSS as the ground plane of a patch antenna, the transmission property with respect to frequency needs to be known.

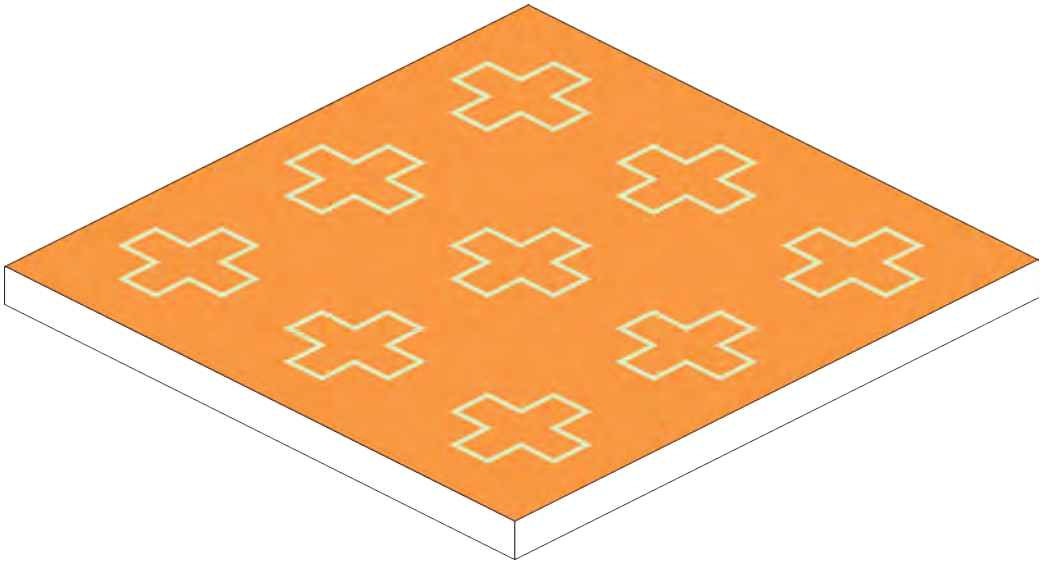

Figure 7.3: Array of loaded element on FR4 substrate

Figure 7.3 shows the possible configuration of an array of loaded elements fabricated on a FR4 substrate. The array was simulated using Ansoft Designer 4 software to know its transmission properties. Since the resonance frequency of the elements vary with their dimension, their dimension were varied and the resulting Transmission Coefficient was obtained.

Figure 7.5 shows transmission coefficient coefficients of different patch size. Neglecting heating loss, the total transmission and reflection coefficient is unity, so the ground plane should be able to reflect the two side bands of a triband patch antenna while suppressing the middle band.

Figure 7.5 shows the center frequency of the reflection band for the loaded element FSS. The element size for the same band in FSS is smaller compared to the hexagonal fractal dimensions.

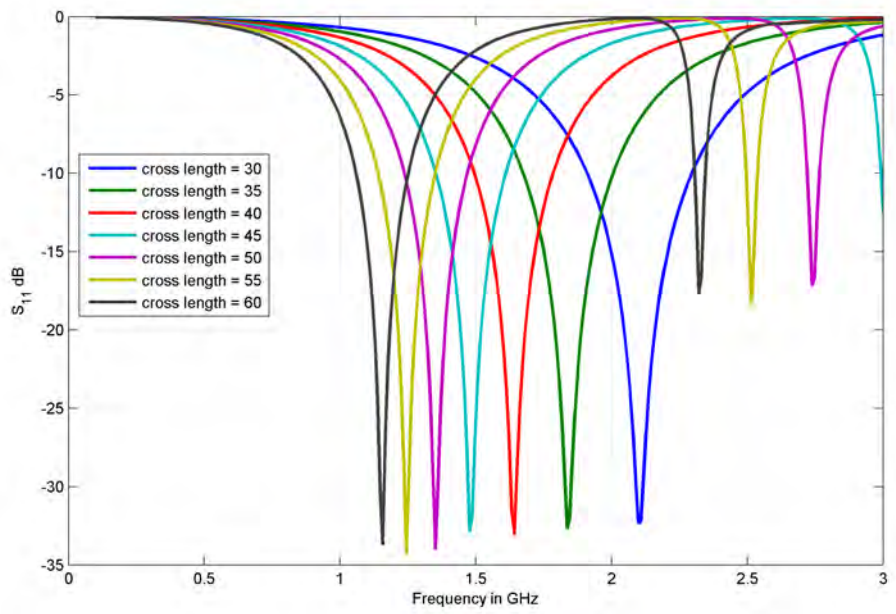

Figure 7.4: Transmission Coefficient of array of loaded element on FR4 substrate

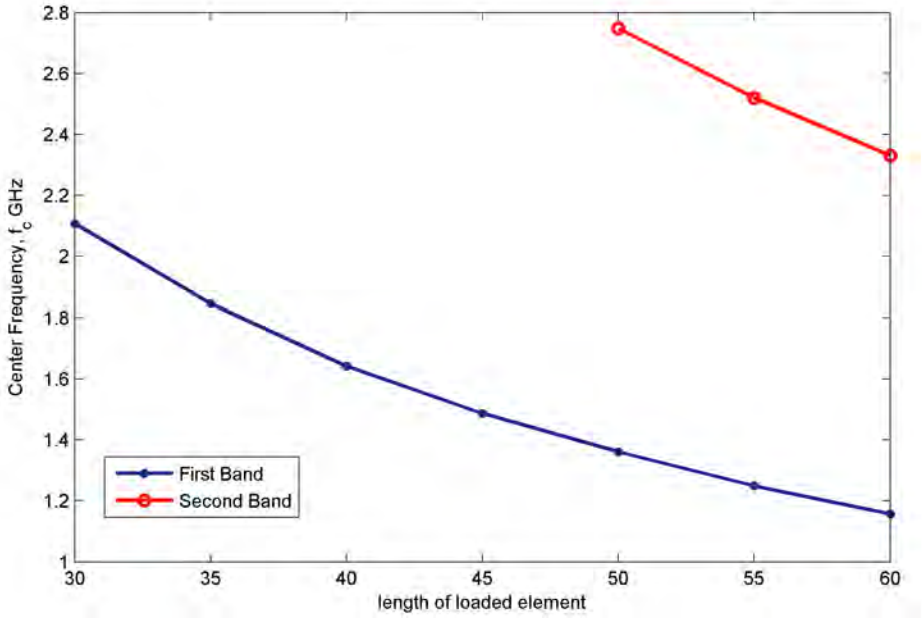

Figure 7.5: Transmission Coefficient of array of loaded element on FR4 substrate

7.4 Second Iteration of Hexaflake Patch with FSS Ground Plane

A second iteration of hexaflake fractal structure with side length of $70mm$ was simulated to observe the effect of adding FSS ground plane. To block the mid operating bands of the antenna, the length of four legged loaded element of the FSS ground plane was found to be $34mm$. The four legged loaded element array was etched off from the metallic ground plane

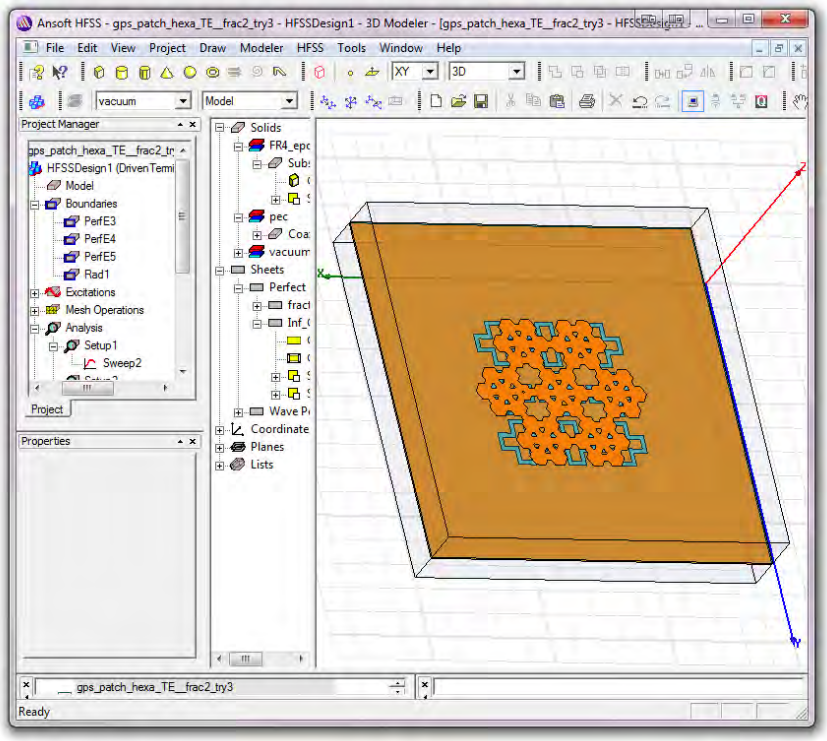

Figure 7.6: Simulation of Second Iteration of Hexaflake Patch with FSS Ground Plane

Figure 7.6 shows the simulation configuration of the patch in Ansoft HFSS. To understand the effect of the addition of FSS substrate, the return loss for a second iteration of hexaflake patch for both with and without an FSS ground plane is plotted in Figure 7.7.

In the figure, the Mid bands of the second iteration of hexaflake patch antenna were suppressed. An interesting effect that can be observed here is that the first band center frequency of the second iteration of hexaflake patch is further reduced from 0.55GHz to 0.23GHz. This change in frequency is unexpected according to

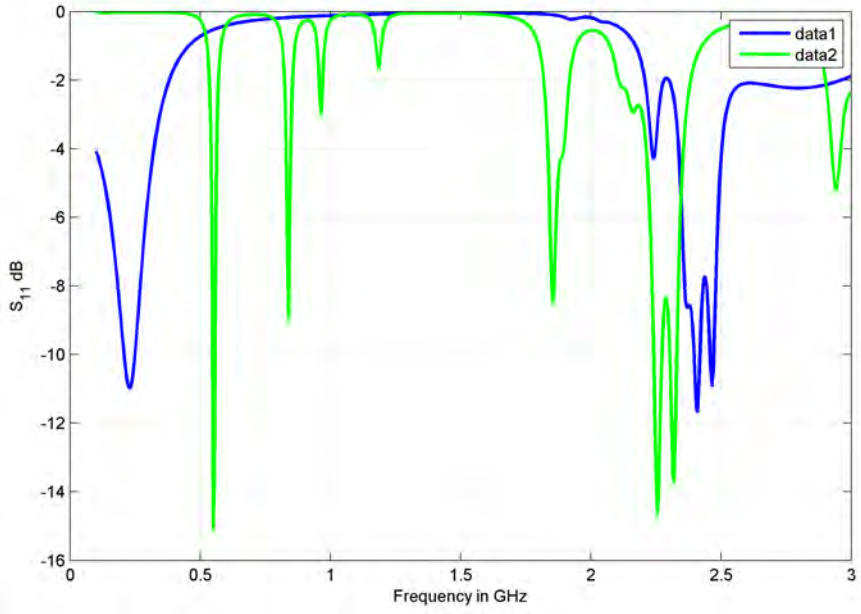

Figure 7.7: Simulation of Second Iteration of Hexaflake Patch with FSS Ground Plane

cavity model.

7.5 Conclusion

In this chapter the effect of introducing a Frequency Selective Surface ground plane on a hexaflake fractal is studied. The application of FSS can suppress frequency bands and also change the resonance frequency of the patch antenna. It would be of further interest if this change of frequency can be modeled analytically.

Chapter 8

Results and Discussion

8.1 Introduction

To compare the three proposed designs, three patch antennas based on the hexaflake structure, first iteration of hexaflake and second iteration of hexaflake were designed and their performance was determined through simulation. The design was done so that the antennas could operate at the L1 frequency band [31] of Global Positioning System. L1 band has a center frequency of 1.57542 GHz.

8.2 Performance of Designed Antenna

8.2.1 As a Hexagonal Patch

For the designed hexagonal patch antenna, the patch size was found to be $59.3mm$. The return loss for the antenna is shown in figure 8.1. The antenna exhibits a single band. The center frequency of the band is 1.5863GHz.

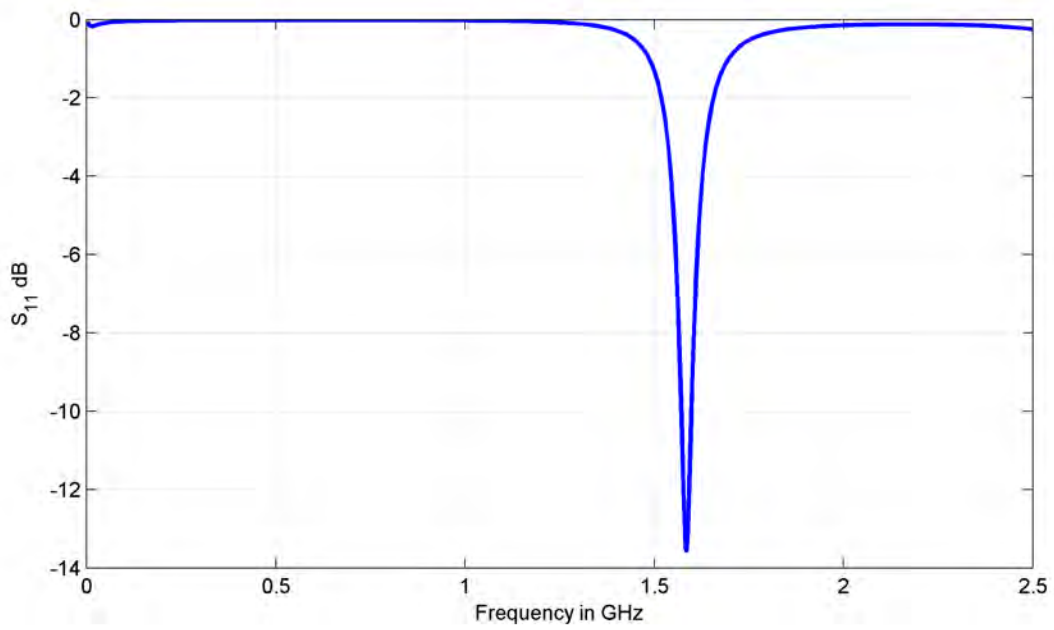

Figure 8.1: Return loss for designed Basic Hexagonal Patch

Figure 8.2 shows the directivity of the antenna with $\phi = 0$ and $\phi = 90°$. Figure 8.3 shows the 3D radiation pattern of the basic hexaflake antenna. The radiation pattern exhibits high directivity at $\theta = 30°$. It can be seen that the radiation pattern has a null at $\theta = 0°$. The 30° main beams have fairly large beam width at upto the back side of the antenna, and thus can work as omnidirectional antenna.

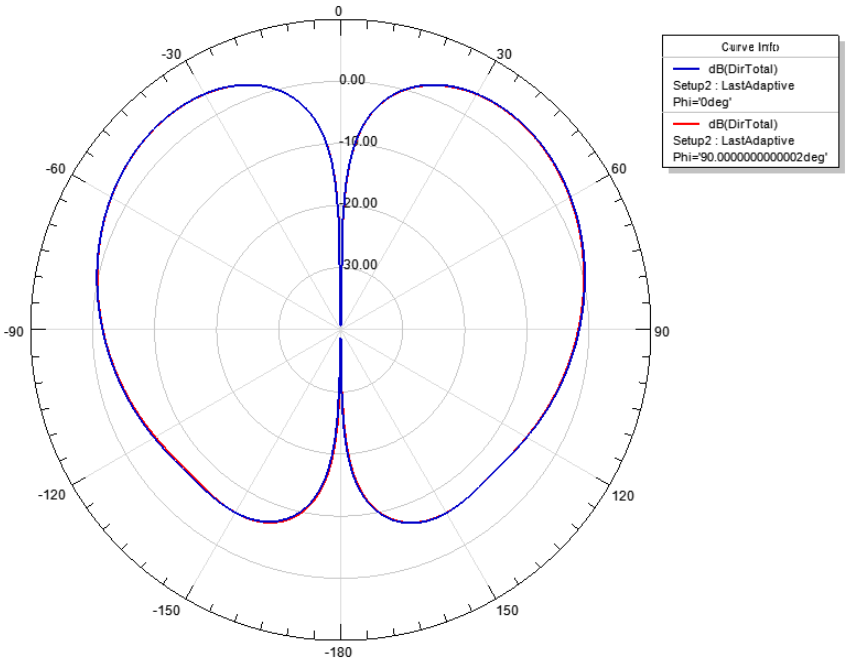

Figure 8.2: Radiation pattern of designed Basic Hexagonal Patch

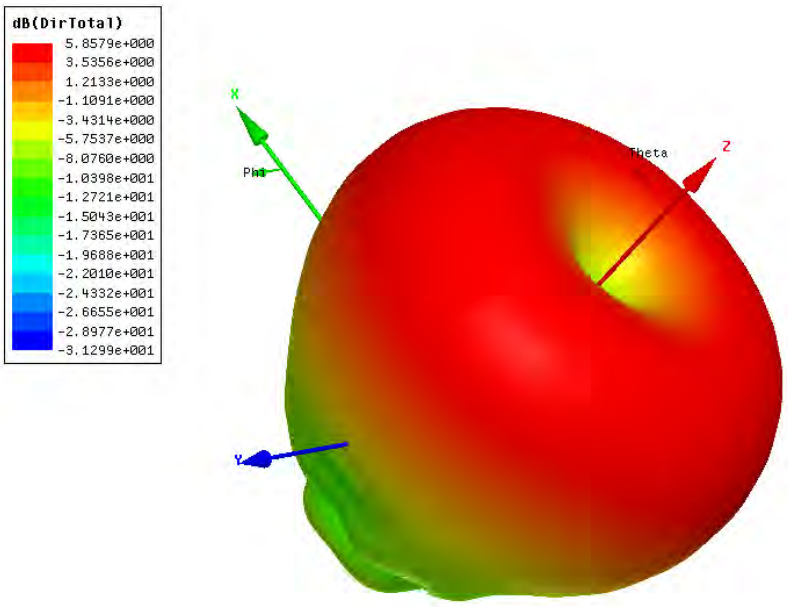

Figure 8.3: 3D Radiation pattern of designed Basic Hexagonal Patch

8.2.2 As a First Iteration of Hexaflake Patch

For the designed first iteration of hexaflake fractal patch antenna, the patch size was found to be $43.2mm$. This size is lower compared to the hexagonal patch structure described above. The return loss for the antenna is shown in figure 8.4. From the figure it can be seen that the antenna has two usable frequency bands that has center frequency at 1.5738GHz and 1.8500GHz.

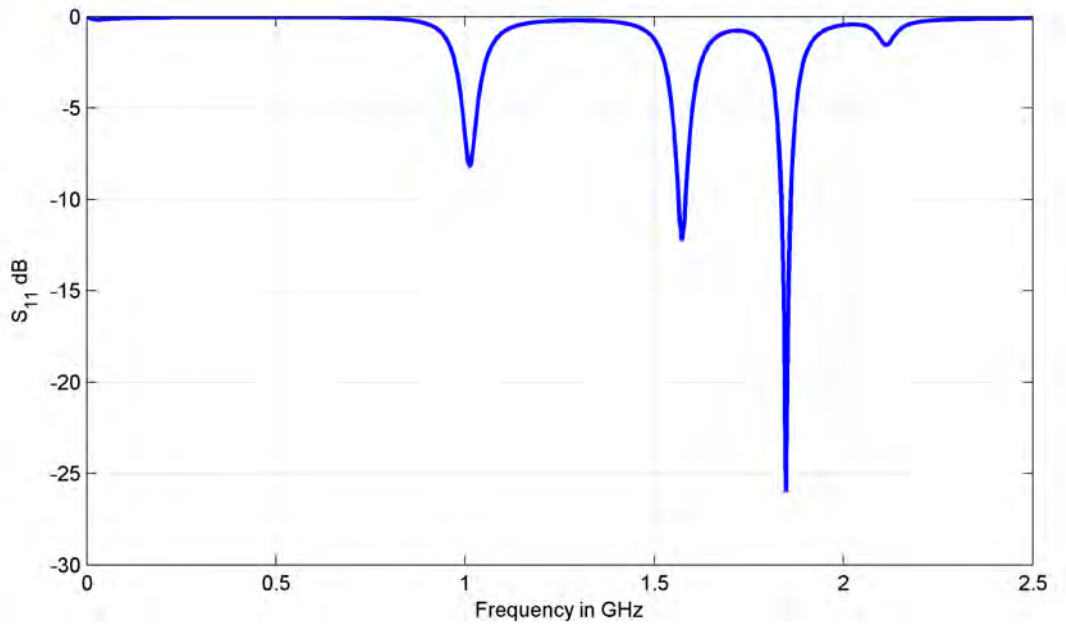

Figure 8.4: Return loss for designed First Iteration of Hexaflake Patch

The frequency band centered at 1.85GHz has a higher frequency compared to the designed 1.575 GHz band.

Figure 8.5 shows the directivity of the antenna with $\phi = 0$ and $\phi = 90°$. Figure 8.6 shows the 3D radiation pattern of the basic hexaflake antenna. Pattern is similar to the basic hexagonal patch antenna pattern, but it is a bit less symmetric. This can be explained by the position of the feed that was chosen to be optimal as opposed to the center fed hexagonal patch. The radiation pattern exhibits high directivity at $\theta = 30°$. The radiation pattern has minimum gain at $\theta = 180°$. But compared to the hexagonal patch, it is less directional, as the null at $\theta = 0°$ exhibits $-15dB$ directivity.

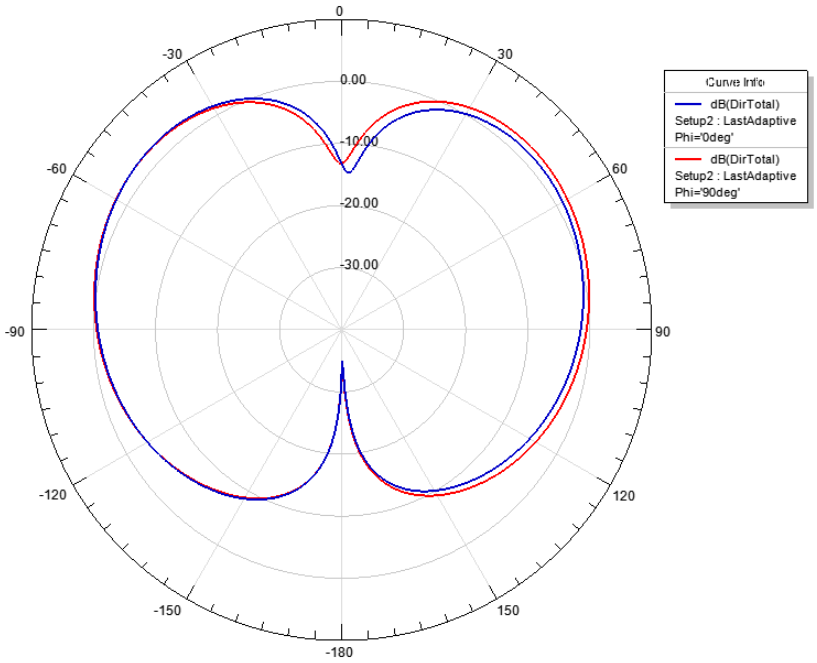

Figure 8.5: Radiation pattern of designed First Iteration of Hexaflake Patch

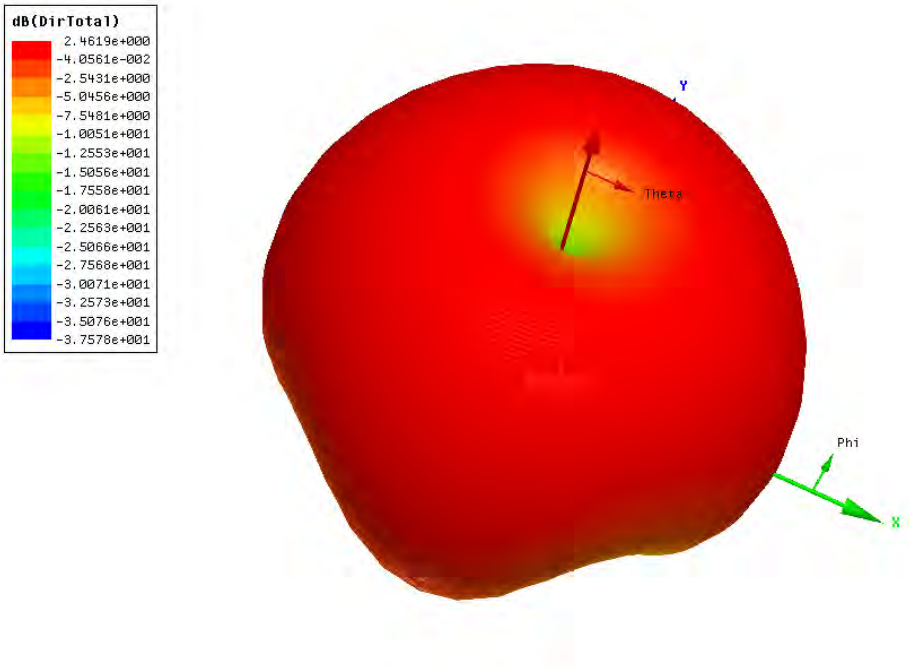

Figure 8.6: 3D Radiation pattern of designed First Iteration of Hexaflake Patch

8.2.3 As a Second Iteration of Hexaflake Patch

For the designed second iteration of hexaflake fractal patch antenna, the patch size was found to be 14.73mm. At this dimension, the patch is so small that it is difficult to couple the elements and antenna feed. As a result, no operatable RL bandwidth is obtained at this frequency. So the second iteration of hexaflake fractal is designed so that the second band of the fractal matches the design frequency. The patch size for this consideration is found to be 39.0mm. This size is also lower compared to both the hexagonal patch structure and the first iteration of hexaflake fractal patch structure described above. The return loss for the antenna is shown in figure 8.7. From the figure it can be seen that the antenna has two usable frequency bands that has center frequency at 1.0250GHz and 1.5750GHz.

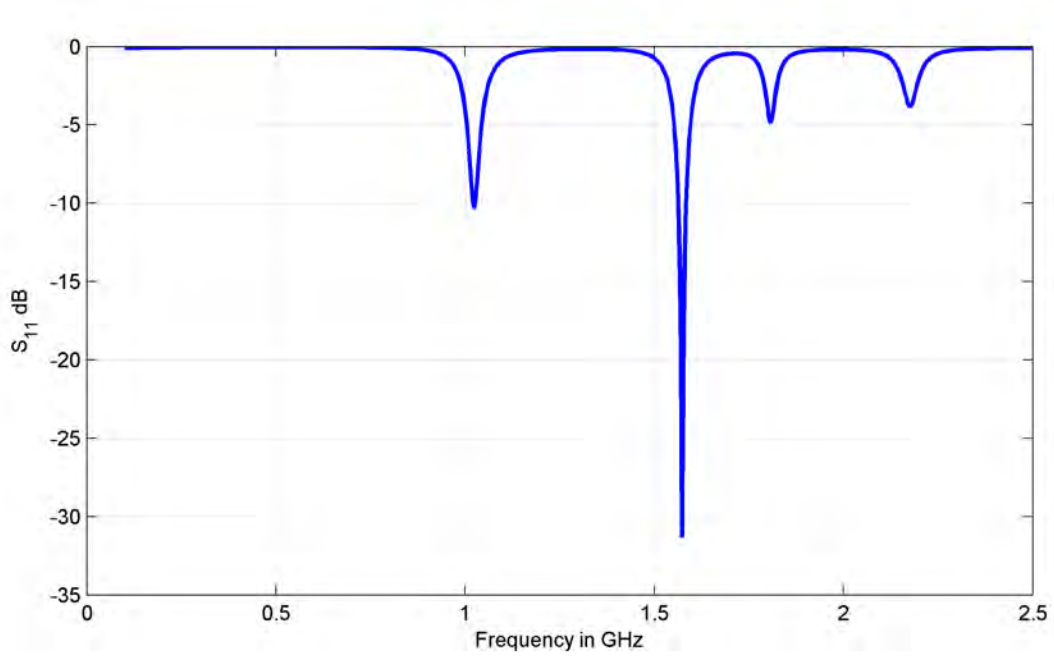

Figure 8.7: Return loss for designed Second Iteration of Hexaflake Patch

Figure 8.8 shows the directivity of the antenna with $\phi = 0$ and $\phi = 90°$. Figure 8.6 shows the 3D radiation pattern of the basic hexaflake antenna. The radiation patterns are similar to the first iteration of hexaflake fractal structure, exhibiting more distortion. The patterns at the E and H plane of the antenna also are significantly more distorted.

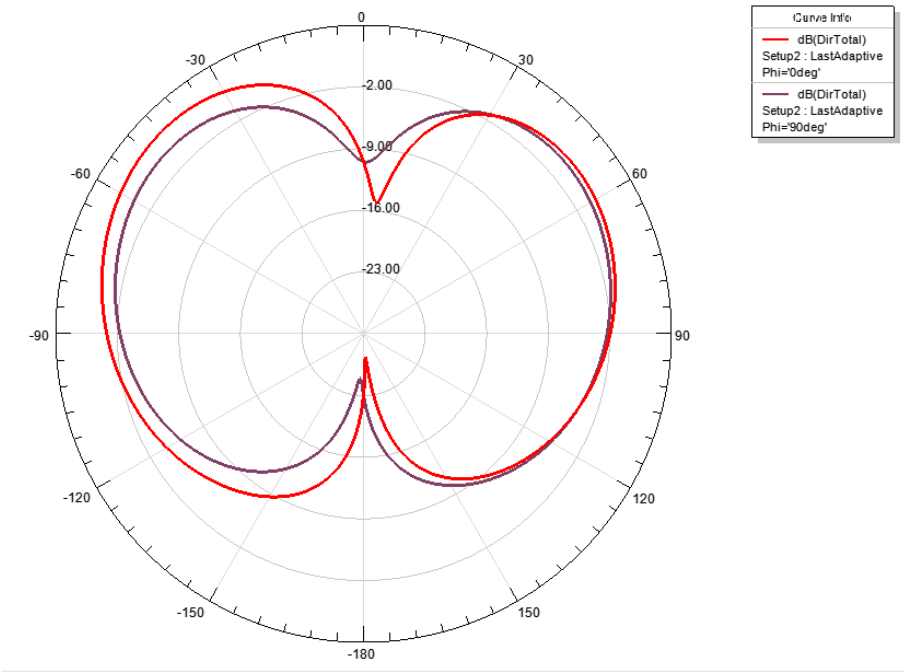

Figure 8.8: Radiation pattern of designed Second Iteration of Hexaflake Patch

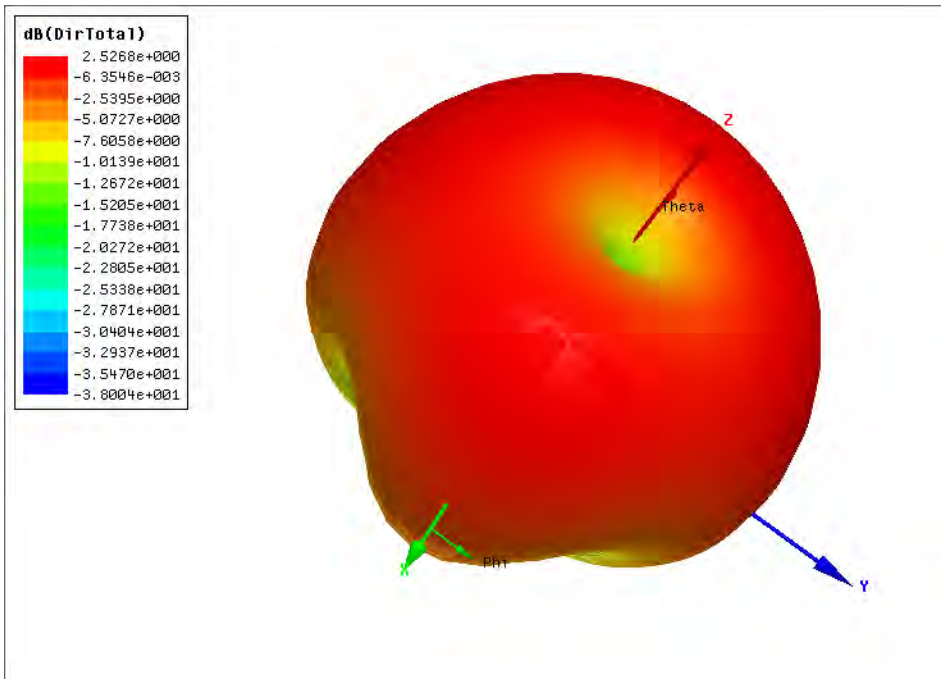

Figure 8.9: 3D Radiation pattern of designed Second Iteration of Hexaflake Patch

8.3 Comparison of Performance

8.3.1 Return Loss

Figure 8.10 shows the radiation pattern of the hexagonal patch, first iteration of hexaflake and second iteration of hexaflake patch at once. The second band First iteration of hexaflake has a higher frequency, but more bandwidth to it. The second iteration has a usable band at a lower frequency, but the RL bandwidth is small.

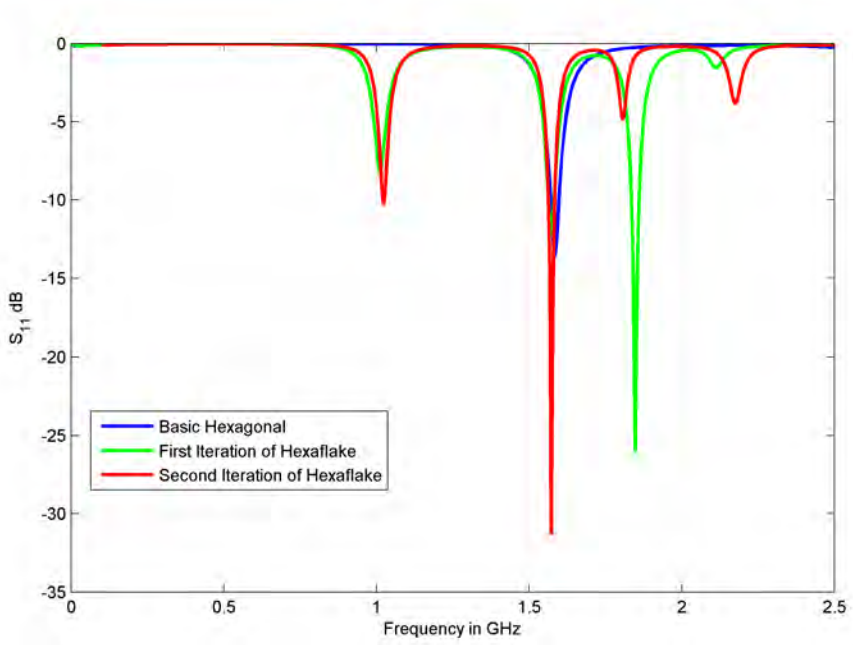

Figure 8.10: Return loss for three designed antennas

8.3.2 Parameters of Antenna

Table 8.1 shows over all comparison of the three designed antennas. The Hexagonal patch element is the largest for the same band frequency, while the first and second iteration of hexaflake fractals give smaller patch size. The first iteration of hexaflake fractal results in a reduction of 27.15% side length compared to the hexagonal patch element, thus 46.92% reduction of patch area. The second iteration of hexaflake fractal patch element results in a reduction of side length of 9.72% reduction of size length, and thus 18.5% reduction of patch area compared to the first iteration of hexaflake fractal, and 34.23% reduction of side length and 56.74% reduction of side length compared to the hexagonal patch element. As the designed antennas all had specified center frequency close to the L1 band of GPS signals, the first and second iteration of hexaflake fractals gave additional bands of operation. The bandwidth

Table 8.1: Comparison of the designed antennas

	Hexagonal Patch	First Iteration of Hexaflake Patch	Second Iteration of Hexaflake Patch
Patch Size (mm)	59.3	43.2	39
Designed Center Frequency (GHz)	1.5863	1.5738	1.575
Percent RL Bandwidth at Center Frequency Band	1.7336	1.112	1.2698
Additional band center frequency (GHz)	-	1.85	1.025
Percent RL Bandwidth at Secondary Band	-	1.3514	0.4878
Peak Directivity	2.5074	1.7628	1.7893
Peak Gain	0.69032	0.14754	0.089227
Front to Back Ratio	1.0473	9.2929	10.002
Radiation Efficiency	0.27531	0.0837	0.04986

is reduced as the fractals are formed compared to the hexagonal patch structure. The second iteration of hexaflake fractal has a lower operating frequency compared to the designed band, but the percentage bandwidth at this band is further reduced due to the smaller dimension of the small hexagonal elements that make up the fractal structure. Both the first and second fractals are less directive compared to the basic hexagonal patch element, and has lower peak gain and radiation efficiency compared to the basic hexagonal element.

8.4 Comparison with other fractal structures

It is difficult to directly compare the patch size of the FR-4 substrate hexaflake patch with the other published results directly, since each of the fractal antennas are designed with a seperate design goal. Different fractal structures such as Koch fractal island patch [6], combined koch and sierpinski fractal patch [32], Pythagoras tree patch [7], Compact Koch patch [14] and patch with Koch shaped fractal defect [15] has been compared to the second iteration of hexaflake fractal patch. For each formentioned published work, the patch size is compared to a possible second iteration of hexaflake patch size that has same resonance frequency. Table 8.2 shows the comparison results. It can be seen that the patch area is reduced compared to most of the fractals studied [6, 7, 14, 32]. In case of patch with Koch shape defect the patch size is smaller compared to second iteration of hexaflake patch structure,

Table 8.2: Comparison of second iteration of hexaflake patch with other published results

Ref	Fractal	Dimension of Patch	Resonance Frequency f_c	Dimension of Equivalent Second Iteration of Hexaflake patch in f_c	Ratio of Second iteration of hexaflake patch area to ref. patch area
Kim (2002) et al. [6]	Koch Fractal Island (Iteration 2)	80.6 x 80.6 ($6496.36mm^2$)	1.173	30.33mm side hexagon slotted ($4779.986mm^2 area$) (first band)	73.57%
Chen et al. [32]	Combined Koch and Sierpinski Fractal	125.5 x 125.5 ($15750.25mm^2$)	0.73375	53.92mm side hexagon slotted ($15108.46mm^2$ area) (first band)	95.92%
Agarwal et al. [7]	Pythagoras tree	63.34 x 63.34 ($4011.95mm^2$)	2.4	14.813 mm side hexagon slotted $1140.15mm^2$ (second band)	28.42%
Oliveria et al. [14]	Compact Koch	29.09 x 37.23 ($1083.02mm^2$)	2.45	13.675 mm side hexagon slotted ($971.638mm^2$)	89.71%
Tiwari et al. [15]	Koch Shaped Fractal Defect	40.1 x 23.12 ($927.112mm^2$)	2.4	14.813 mm side hexagon slotted $1140.15mm^2$ (second band)	122.90%

so it might be interesting to know if the introduction of fractal shape defects in hexaflake fractals can produce smaller center frequency.

8.5 Conclusion

In this chapter, the performance of the designed fractal antennas are evaluated. The three designed antennas are compared to each other and the effect of introducing fractal iterations to hexagonal patch structure is explored. It was found that fractal structure reduced the patch size with some trade off in antenna radiation efficiency.

Chapter 9

Conclusions

9.1 Concluding Remarks

In this thesis, the first and second iteration of hexaflake fractal structures have been explored as possible patch antenna structures. The basic hexagonal structure is also studied as a patch antenna element. An analytic model for explaining radiation properties of a hexagonal patch element has been derived. Finite Element Method was used to obtain the final performance parameters of the antenna, as it is more accurate compared to the simplified model.

The first iteration of hexaflake fractal results in a reduction of 46.92% patch area compared to hexagonal patch element. The second iteration of hexaflake fractal patch element results in 18.5% reduction of patch area compared to the first iteration of hexaflake fractal, and 56.74% reduction of patch area compared to the hexagonal patch. In turns, the hexagonal patch reduces the patch size compared to rectangular patch element, and thus the fractal structures clearly demonstrate ability to reduce patch size.

9.2 Recommendation for Future Work

There are number of scopes to extend the research done in the thesis. Some possible areas are:

- The multiport analysis model discussed can be further improved to incorporate the mutual coupling between adjacent slots of the hexagonal fractals.
- The filter can be fabricated and measured data can be obtained to be compared with the simulated results
- Effect of hybrid fractal structures based on hexaflake and other fractal structures can be studied to improve radiation efficiency of the fractal patch antenna.
- The effect of introducing FSS can be modelled for frequency change by modified transmission line model.

References

[1] Mandelbrot, B. *The Fractal Geometry of Nature*. W.H. Freeman and Company, 1982

[2] Pickover, C.A. *The Math Book: From Pythagoras to the 57th Dimension, 250 Milestones in the History of Mathematics*. Sterling Publishing Company, 2009

[3] Cohen, N. "Fractals' new era in military antenna design." *Journal of RF Design*, volume 1, 2005

[4] Dennis, K. "Sierpinski n-gons." Technical report, Michigan State University, MI, 1999

[5] Puente, C., Romeu, J., Pous, R., Garcia, X. and Benitez, F. "Fractal multiband antenna based on the sierpinski gasket." *Electronics Letters*, volume 32, no. 1:pp. 1–2, 1996

[6] Kim, I.K., Yook, J.G. and Park, H.K. "Fractal-shape small size microstrip patch antenna." *Microwave And Optical Technology Letters*, volume 34:pp. 15–17, 2002

[7] Aggarwal, A. and Kartikeyan, M.V. "Pythagoras tree: A fractal patch antenna for multi-frequency and ultra-wide band-width operations." *Progress In Electromagnetic Research C*, volume 16:pp. 25–35, 2010

[8] Tiwari, A. and Kumar, R. "On the design of cpw-fed appollian gasket fractal antenna." In "Progress In Electromagnetics Research Symposium Proceedings, Moscow, Russia," , 2009

[9] Mahatthanajatuphat, C. and P., A. "A bidirectional multiband antenna with modified fractal slot fed by cpw." *Progress In Electromagnetics Research, PIER*, volume 95:pp. 59–72, 2009

[10] Mahatthanajatuphat, C., Saleekaw, S. and Akkaraekthalin, P. "A rhombic patch monopole antenna with modified minkowski fractal geometry for umts, wlan, and mobile wimax application." *Progress In Electromagnetics Research, PIER*, volume 89:pp. 57–74, 2009

[11] Yu, Z.W., Wang, G.M., Gao, X.J. and Lu, K. "A novel small-size single patch microstrip antenna based on koch and sierpinski fractal-shapes." *Progress In Electromagnetics Research Letters*, volume 17:pp. 95–103, 2010

[12] Hazdra, P. and Mazanek, M. "The miniature fractal patch antenna." In "Radioelektronika 2005 Conference Proceedings," , 2005

[13] Prombutr, N. and Akkaraaektharin, P. "Analysis and design hilbert curve fractal antenna feed with co-planar waveguide for multi-band wireless communications." *International Journal of Engineering,*, volume 2, 2008

[14] Oliveira, E.E.C., D'Assuncao, A.G., de Andrade Martins, R. and Campos, A.L.P.S. "A new compact koch fractal patch antenna on an ebg ground plane." In "Proc. Int Antenna Technology (iWAT) Workshop," pp. 1–4, 2010

[15] Tiwari, H. and Kartikeyan, M.V. "A staked microstrip patch antenna with fractal shaped defectd." *Progress In Electromagnetics Research C*, volume 14:pp. 185–195, 2010

[16] Chakraborty, U., Chatterjee, S., Chowdhury, S.K. and Sarkar, P.P. "A compact microstrip patch antenna for wireless communication." *Progress In Electromagnetics Research C,*, volume 18:pp. 211–220, 2011

[17] Yang, S.S.L. and Luk, K.M. "Wideband hexagonal-shape stacked-patch antenna array with l-probe feed." *Microwave And Optical Technology Letters*, volume 43:pp. 77–79, 2004

[18] Balanis, C.A. *Antenna Theory Analysis and Design*. John Wiley & Sons, 1997

[19] Fang, D.G. *Antenna theory and microstrip antennas*. CRC Press, 2010

[20] James, J.R. and Hall, P.S. *Handbook of Microstrip Antennas*. Peter Peregrinus Ltd., London, 1989

[21] Kumar, G. and Ray, K.P. *Broadband Microstrip Antennas*. Artech House, 2003

[22] Garg, R., Bhartia, P., Bahl, I. and Ittipiboon, A. *Microstrip Antenna Design Handbook*. Artech House Inc., 2001

[23] Derneryd, A. "Linearly polarized microstrip antennas." *Antennas and Propagation, IEEE Transactions on*, volume 24, no. 6:pp. 846–851, 1976

[24] Gupta, K.C. *Handbook of Microstrip Antennas*, chapter Multiport network approach for modelling and analysis of microstrip patch antennas and arrays, pp. 455–522. Peter Peregrinus Ltd., 1989

[25] Benalla, A. and Gupta, K.C. "Faster computation of z-matrices for rectangular segments in planar microstrip circuits (short paper)." *Microwave Theory and Techniques, IEEE Transactions on*, volume 34, no. 6:pp. 733–736, 1986

[26] Lee, S.H., Benalla, A., , and Gupta, K.C. "Faster computation of z-matrices for triangular segments in planar circuits." *Inrernational Journal of Microwave and Millimeter-Wave Computer-Aided Engineering*, volume 2:pp. 98–107, 1992

[27] Guo, C., Sun, H. and Lu, X. "A novel dual dualband frequency selective surface with periodic cell perturbation." *Progress In Electromagnetics Research B*, volume 9:p. 137149, 2008

[28] Lee, Y.J., Yeo, J., Mittra, R. and Park, W.S. "Design of a high-directivity electromagnetic band gap (ebg) resonator antenna using a frequency-selective surface (fss) superstrate." *Microwave And Optical Technology Letters*, volume 43, 2004

[29] Munk, B.A. *Frequency Selective Surfaces*. Wiley, 2000

[30] Choudhury, S.M., Zaman, M.A., Gaffar, M. and Matin, M.A. "A novel approach for changing bandwidth of fss filter using gradual circumferential variation of loaded elements." In "Proc. of Progress in Electromagnetic Research Symposium," , 2010

[31] Do, J., Akos, D.M. and Enge, P.K. "L and s bands spectrum survey in the san francisco bay area." In "Proc. Position Location and Navigation Symp. PLANS 2004," pp. 566–572, 2004

[32] Chen, W.L., Wang, G.M. and Zhang, C.X. "Small-size microstrip patch antennas combining koch and sierpinski fractal-shapes." *Antennas and Wireless Propagation Letters, IEEE*, volume 7:pp. 738–741, 2008